


5-2018

Effects of Hydration and Mineralization on the Mechanical Behavior of Collagen Fibrils

Marco Fielder
University of Arkansas, Fayetteville

Follow this and additional works at: <https://scholarworks.uark.edu/etd>

 Part of the [Biomechanical Engineering Commons](#), [Biomechanics and Biotransport Commons](#), and the [Nanoscience and Nanotechnology Commons](#)

Citation

Fielder, M. (2018). Effects of Hydration and Mineralization on the Mechanical Behavior of Collagen Fibrils. *Graduate Theses and Dissertations* Retrieved from <https://scholarworks.uark.edu/etd/2795>

This Thesis is brought to you for free and open access by ScholarWorks@UARK. It has been accepted for inclusion in Graduate Theses and Dissertations by an authorized administrator of ScholarWorks@UARK. For more information, please contact scholar@uark.edu, uarepos@uark.edu.

Effects of Hydration and Intrafibrillar Mineralization on the Mechanical Behavior of
Collagen Fibrils

A thesis submitted in partial fulfillment
of the requirements for the degree of
Master of Science in Microelectronics-Photonics

by

Marco Fielder
Hastings College
Bachelor of Arts in Physics, 2016

May 2018
University of Arkansas

This thesis is approved for recommendation to the Graduate Council.

Arun K. Nair, Ph.D.
Thesis Director

Uchechukwu Wejinya, Ph.D.
Committee Member

Jingyi Chen, Ph.D.
Committee Member

Rick Wise, Ph.D.
Ex-Officio Member

The following signatories attest that all software used in this thesis was legally licensed for use by Marco Fielder for research purposes and publication.

Mr. Marco Fielder, Student

Dr. Arun K. Nair, Thesis Director

This thesis was submitted to <http://www.turnitin.com> for plagiarism review by the TurnItIn company's software. The signatories have examined the report on this thesis that was returned by TurnItIn and attest that, in their opinion, the items highlighted by the software are incidental to common usage and are not plagiarized material.

Dr. Rick Wise, Program Director

Dr. Arun K. Nair, Thesis Director

Abstract

Bone is a composite biomaterial with a structural load-bearing function. Understanding the biomechanics of bone is important for characterizing factors such as age, trauma, or disease, and in the development of scaffolds for tissue engineering and bioinspired materials. At the nanoscale, bone is primarily composed of collagen protein, apatite crystals, and water. Though several studies have characterized nanoscale bone mechanics as the mineral content changes, the effect of water, mineral, and carbon nanotube (CNT) content and distribution in fibril gap and overlap regions is unexplored. This study used molecular dynamics to investigate the change in collagen fibril deformation mechanisms as a function of mineral, water, and CNT content. Collagen fibrils with 0 wt%, 20 wt%, and 40 wt% intrafibrillar mineralization and 0 wt%, 2 wt%, and 4 wt% hydration were studied under tension and compression. Non-mineralized fibrils with 43 wt% water and 5 wt%, 10 wt%, and 15 wt% CNTs were studied under compression.

An increase in mineral content for hydrated fibrils was found to reduce the nonlinear stress versus strain behavior caused by hydration, and the Young's modulus of non-mineralized and mineralized fibrils decreased as the water content increased. At low water contents, it was found in non-mineralized fibrils that water primarily occupied voids in the gap regions, while in mineralized fibrils water primarily occupied voids in the overlap regions. Mineral and water content were found to affect the distribution of water in fibrils in tension and compression, which changed the deformation behavior of the gap and overlap regions. An increase in water content was found to increase the gap/overlap ratio by approximately 40% in non-mineralized fibrils and 16% in mineralized fibrils. For non-mineralized fibrils it was found that the gap/overlap ratio increased with an increase in tensile or compressive stress, while in mineralized fibrils the gap/overlap ratio decreased with an increase in stress. CNTs in non-mineralized fibril gap region voids reduced the decrease in the gap/overlap ratio as stress increased. CNTs increased the non-mineralized fibril elastic modulus from 0.43 GPa to

approximately 1.74 GPa to 2.83 GPa, which was comparable to the elastic moduli of mineralized fibrils.

Acknowledgements

I would like to acknowledge and thank support from my advisor Dr. Arun K. Nair, and my colleagues and friends in the Multiscale Materials Modeling Laboratory. I would also like to acknowledge and thank Dr. Rick Wise, Renee Hearon, and the friends I've made in the Microelectronics-Photonics Graduate Program. You have all helped me in developing and conducting this study, and for guiding me in becoming a better and more knowledgeable person and scientist.

This thesis was also supported by the Department of Mechanical Engineering at the University of Arkansas, the Arkansas High Performance Computing Center (AHPCC), and by the National Science Foundation under the grants ARI# 0722625, MRI# 0959124, # 0963249, and #0918970, and a grant from the Arkansas Economic Development Commission and the University of Arkansas Office of the Vice Provost for Research and Innovation.

Dedication

This thesis is dedicated to my parents, Jim Fielder and Monica Fielder, for their encouragement and support of me before and during my time at the University of Arkansas Graduate School, and for which I am supremely thankful.

Table of Contents

Chapter 1: Introduction.....	1
1.1 Background and Literature Review.....	1
1.2 Objectives	5
Chapter 2: Materials And Methods.....	7
2.1 Molecular Dynamics.....	7
2.2 CHARMM Interatomic Potential.....	8
2.3 Fibril Models of Varying Mineral and Water Content.....	9
2.4 Tensile and Compressive Tests and Analysis of Deformation Mechanisms.....	12
2.5 Collagen Fibril and Carbon Nanotube Composites.....	13
Chapter 3: Results.....	15
3.1 Fibril Tensile Tests.....	15
3.2 Fibril Compressive Tests.....	26
3.3 Carbon Nanotube Tensile and Compressive Tests.....	36
3.4 Fibrils with CNTs Compressive Tests.....	38
Chapter 4: Conclusions	43
References.....	46
Appendix A: Description of Research for Popular Publication.....	52
Appendix B: Executive Summary of Newly Created Intellectual Property.....	54
Appendix C: Potential Patent and Commercialization Aspects of Intellectual Property.....	55
Appendix D: Broader Impact of Research.....	56
Appendix E: Microsoft Project for Microelectronics-Photonics Degree Plan.....	57
Appendix F: Identification of Software Used in Research and Thesis.....	58

Appendix G: All Publications Published, Submitted, and Planned.....59

List of Figures

Figure 1.1.1 Schematic representing the hierarchical structure of compact bone.....	3
Figure 1.1.2 A collagen fibril visualized as a schematic.....	4
Figure 1.1.3 Schematic showing the chirality vectors of carbon nanotube geometry.....	4
Figure 2.2.1 Collagen fibrils visualized with varying mineral and water contents.....	11
Figure 3.1.1 Tensile stress vs. strain of collagen fibrils.....	16
Figure 3.1.2 The tensile Young's modulus vs. fibril water content.....	17
Figure 3.1.3 The tensile Young's modulus vs. fibril mineral content.....	20
Figure 3.1.4 Fibril gap and overlap regions visualized in a schematic.....	21
Figure 3.1.5 Gap/overlap ratio vs. tensile stress for non-mineralized fibrils.....	22
Figure 3.1.6 Gap/overlap ratio vs. tensile stress for 20% mineralized fibrils.....	23
Figure 3.1.7 Gap/overlap ratio vs. tensile stress for 40% mineralized fibrils.....	25
Figure 3.2.1 Compressive stress vs. strain of collagen fibrils.....	26
Figure 3.2.2 The compressive Young's modulus vs. fibril water content.....	28
Figure 3.2.3 The compressive Young's modulus vs. fibril mineral content.....	30
Figure 3.2.4 Gap/overlap ratio vs. compressive stress for non-mineralized fibrils.....	32
Figure 3.2.5 Gap/overlap ratio vs. compressive stress for 20% mineralized fibrils.....	33
Figure 3.2.6 Gap/overlap ratio vs. compressive stress for 40% mineralized fibrils.....	35
Figure 3.3.1 Tensile stress vs. strain of a carbon nanotube.....	36
Figure 3.3.2 Compressive stress vs. strain of carbon nanotubes.....	37
Figure 3.4.1 Collagen fibrils with CNTs in the gap regions.....	38
Figure 3.4.2 Compressive stress vs. strain of fibrils with CNTs.....	39
Figure 3.4.3 The compressive Young's modulus vs. fibril water content.....	40
Figure 3.4.4 Gap/overlap ratio vs. compressive stress of no-mineralized fibrils	41

List of Tables

Table 3.1.1 Tensile Young's moduli obtained by other studies of fibrils.....	18
Table 3.2.1 Compressive Young's moduli obtained by other studies of fibrils.....	29
Table 3.3.1 Tensile Young's moduli of CNTs determined by other studies	37

Chapter 1: Introduction

1.1 Background and Literature Review

Bone is a biological material with the primary function of providing structural and load-bearing support in vertebrate organisms [1]. It is important to study and determine the mechanical properties of bone, since its properties can change due to several factors. For example, mineral and water content in bone have both been found to decrease as a person gets older [2-4]. Bone's mechanical properties also depend on the specific bone's function in the body, which affects bone's stiffness and structure. Genetic disorders can also have drastic effects on bone's properties. For example, osteogenesis imperfecta, also known as brittle bone disease, can cause bones to break more easily [3]. Ehler's-Danlos syndrome is also a genetic disorder that causes joints, skin, and bones to be hyperflexible [5]. Some additional factors that can affect the properties of bone are a person's nutrition, amount of exercise, or injury due to external force. If the mechanical and structural properties of a person's bones can be measured, that information can be used by medical professionals to determine what factors might be affecting that person's bone behavior if the properties of bone for different conditions are quantified. Understanding the structure and mechanical properties of bone is also useful for development of new bio-inspired materials that require a structural or load-bearing function. It has a specific application for the development of scaffolds for bone tissue engineering and medical implants.

A variety of experimental and computational methods have been used to study the mechanical structure and behavior of bone at the microscale and nanoscale. Experimental techniques include x-ray diffraction to determine bone structure at different conformations [6], atomic force microscopy and micromechanical devices to investigate bone stiffness and deformation behavior [7-9], and nuclear magnetic resonance spectroscopy to look at the atomic behavior of bone [10]. Computational methods used to study bone include molecular dynamics simulations [11-16], finite element analysis [17-20], and ab initio methods [21, 22], which can be used to study bone's structure conformations, stiffness,

deformation behavior, and atomic behavior.

Bone is a composite material of approximately 60% apatite mineral, 30% collagen protein, and 10% water [10, 11, 17, 22, 23]. Bone is also hierarchical, with different structures at different size scales [1, 24] which can be seen in Figure 1.1.1. At the visible macroscale, bone is mainly composed of two types of bone structures. The first is cancellous bone, also known as trabecular bone or spongy bone, which is located primarily in the interior of bones and has a random and porous network structure that allows for the presence of fluidic marrow [25]. The other type of bone is cortical bone, also known as compact bone, which is mainly on the exterior shell of bone [26]. Cortical bone is denser and has a more unidirectionally ordered structure compared to cancellous bone, since it has a greater structural load-bearing function.

At the millimeter scale, cortical bone is composed mainly of osteons with haversian canals at the center of individual osteons that allow for other tissues such as vascular or nervous tissue [27]. These haversian canals are then surrounded by multiple concentric layers known as lamella. The osteons are typically a few millimeters long and approximately 200 μm in diameter. Each lamella layer is made up of densely packed, unidirectional collagen fibers. The direction orientation of the collagen fibers between lamella layer differs in order to strengthen the osteon in multiple directions. The collagen fibers are typically around 5 μm in diameter.

The aligned collagen fibers are structured from bundles of collagen fibrils that have a diameter of approximately 10-500 nm and are embedded in an extrafibrillar mineral matrix. A schematic of the fibril structure can be seen in Figure 1.1.2. Collagen fibrils themselves are a composite of collagen protein, intrafibrillar hydroxyapatite mineral, and water. The collagen fibrils have a triclinic structure whereby they arrange themselves in a staggered periodic conformation [28, 29]. Due to this, the collagen molecules form what is known as gap regions between adjacent collagen molecule ends along the fibril length axis. Along the fibril longitudinal axis, the staggered conformation means collagen molecules are not aligned in the longitudinal direction, but align themselves so that the lengths of

adjacent collagen molecules partially overlap, creating what are known as overlap regions. This staggered periodic structure is known as *D*-banding, where *D* is approximately 67 nm and is the combined length of the gap and overlap regions [14, 21].

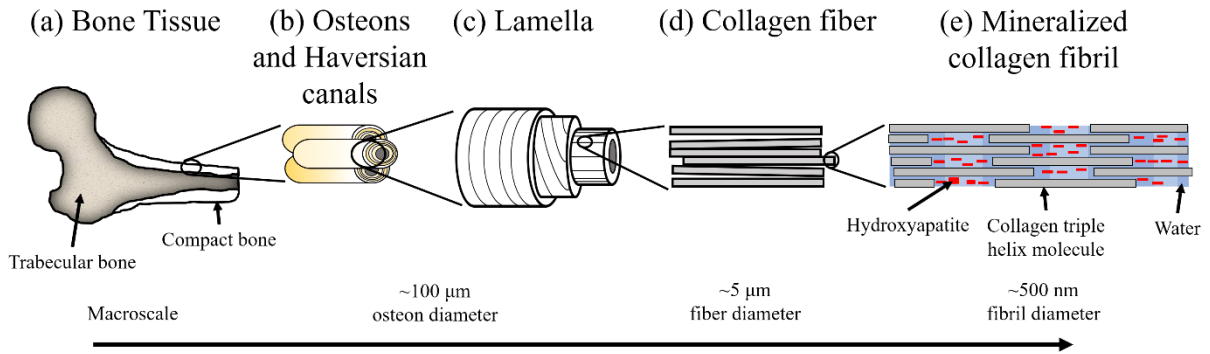


Figure 1.1.1 Schematic representing the hierarchical structure of compact bone. Size scale is in descending order from (a) macroscale bone tissue, to (b) osteons and haversian canals, to (c) lamella, to (d) collagen fibers, to (e) nanoscale collagen fibrils composed of collagen protein molecules (grey), hydroxyapatite mineral (red), and water (blue).

The collagen molecules composing the fibril are primarily type 1 collagen molecules. The collagen molecules have a diameter of approximately 1.5 nm, and are composed of three individual left-handed helical peptides that come together to form a right-handed triple helical collagen molecule. The mineral phase of the fibrils is more brittle than the protein phase of the fibril and is primarily hydroxyapatite (HAP) with a chemical form of $\text{Ca}_{10}(\text{PO}_4)_6(\text{OH})_2$. It has been shown experimentally that the mineral primarily begins to nucleate in the gap regions of the fibril [30, 31]. As the mineral continues to nucleate, mineral within the collagen molecules and in the fibril gap regions is known as intrafibrillar mineral, while the mineral between individual collagen fibrils is known as extrafibrillar mineral. Substitution of the *OH* group in hydroxyapatite can result in the formation of other types of apatite in bone, which typically occurs naturally as a person ages, and can affect the structural and mechanical properties of the bone [3, 10]. Water in the fibril that fills the remaining spaces in the fibril is known as mobile water, while water that is bonded to the collagen or hydroxyapatite is known as structural water [10, 16, 32, 33].

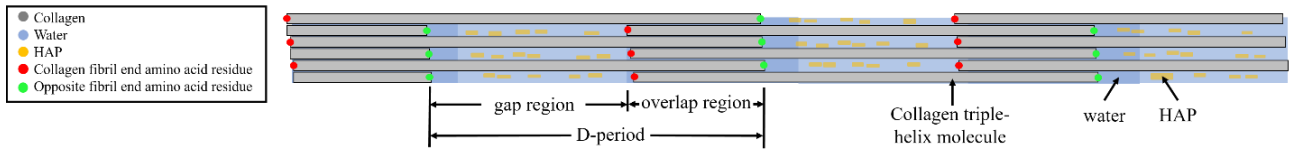


Figure 1.1.2 A collagen fibril visualized as a schematic. The collagen molecule end residues are represented in green and red to highlight the ends of the gap and overlap regions.

Carbon nanotubes are currently being studied as a material to increase the strength of bone and scaffolds for tissue engineering [34-41]. Carbon nanotubes (CNTs) are cylindrical tubes of graphite with an sp^2 bond structure, and are several nanometers in diameter and can be anywhere from several nanometers to several millimeters in length [42]. Their structure is that of conformations of benzene rings that can align themselves differently depending on the type of carbon nanotube structure. The three types of structures of carbon nanotubes are based on the vector direction rolling of the graphite sheet, and is represented as (n,m) integer indices based on the coefficients of the rolling direction vector components as shown in Figure 1.1.3, The vector \mathbf{b} represents the tube axis, while the vectors \mathbf{a}_1 and \mathbf{a}_2 represent the geometry of graphene, and the vector \mathbf{c} is given as $\mathbf{c} = n\mathbf{a}_1 + m\mathbf{a}_2$. “Armchair” carbon nanotubes have the indices (n,n) . “Chiral” carbon nanotubes have the indices of (n,m) where $n \geq 1, m \geq 1$, and $n \neq m$, while “zigzag” carbon nanotubes have the indices of $(n,0)$ [43].

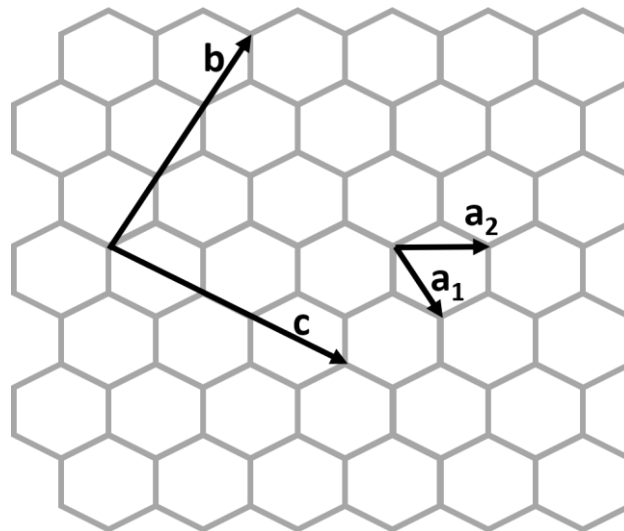


Figure 1.1.3 Schematic showing the chirality vectors describing carbon nanotube geometry.

The diameter (d) of a carbon nanotube is dependent on its indices, and the diameter of the carbon nanotube in nanometers is given by Equation 1.1.1 [43]:

$$d = \left(\frac{0.246}{\pi}\right) \sqrt{(n^2 + m^2 + nm)} \quad (\text{Equation 1.1.1})$$

Carbon nanotubes are typically produced by arc discharge methods, laser ablation, or chemical vapor deposition [42]. Carbon nanotubes may have capped or open ends, and may also come in the conformation of single tubes known as single-walled carbon nanotubes, or as concentric tubes known as multi-walled carbon nanotubes [42, 44]. The shortest carbon nanotube ever made is cycloparaphenylene, and is one benzene ring in length, while the smallest diameter stable carbon nanotube made has a diameter of about 0.4 nm [45]. Carbon nanotubes have been shown to have excellent thermal and electrical conductivity properties [46, 47], as well as effective bio-molecular adsorption properties that have given promise to carbon nanotubes use in drug delivery systems and for use in bio-composites [48]. Carbon nanotubes are also renowned for their remarkable stiffness, and have been found to have a Young's modulus as high as 1 TPa [44], which shows promise for carbon nanotubes as a stand-alone material or use in composites that require a high stiffness or structural integrity.

1.2 Objectives

The purpose of the first part of this study was to observe how the mechanical behavior and properties of collagen fibrils and its constituents at the nanoscale, simulated using molecular dynamics, change as a function of both mineral and water content due to an applied tensile or compressive stress, since bone water content is known to decrease due to increased mineralization [32, 33, 49]. This study investigated the effect of collagen fibril water content on the conformation of mineralized collagen fibrils. To quantify, this study looked at the how the collagen fibril water contents of 0 wt%, 2 wt%, and 4 wt% affect the mechanical behavior of the fibril for degrees of intrafibrillar mineralization of 0 wt%, 20 wt%, and 40 wt%. The reason for looking into the change in the

mechanical properties of bone fibrils due to simultaneous variations in mineral and water content is due to the fact that studies have shown that bone fibril mineral and water content can vary due to different factors, such as age [4]. The results of this part of the study have an impact on the optimization of multi-scale models of bone, and are also important for the creation of new composite materials inspired by bone fibril structure and mechanical behavior, such as scaffolds for tissue engineering, or skeletal implants or prosthetics.

The second part of this study sought to determine the structural and mechanical behavior of collagen fibril-carbon nanotube composites, and if such a composite could mirror the structural and mechanical behavior of mineralized collagen fibrils. The results of this part of the study are important for the creation of new bone scaffolds for tissue engineering.

Chapter 2: Materials and Methods

In this chapter, the materials and methods for the thesis are presented. In Section 2.1, an outline of molecular dynamics (MD) is presented, as well as the justification for the use of MD simulations for this study of collagen fibrils. When utilizing MD, a specific interatomic potential must be selected to accurately describe the energetic interactions between atoms. In Section 2.2, the reason for choosing the CHARMM interatomic potential is presented, as well as a description of the CHARMM potential. In Section 2.3, the development of the fibril model is presented, along with assumptions made of the model. In Section 2.4, the methods for performing the tensile and compressive tests using MD is presented, as well as the methods for analyzing the mechanical behavior of the fibrils. Lastly, in Section 2.5 the development of the model for CNTs is presented, as well as the development of the inclusion of the CNT models into the fibril model.

2.1 Molecular Dynamics

Studying the nanoscale behavior of fibrils and the interaction between fibrils and carbon nanotubes can be difficult using conventional experimental techniques. One method for studying these behaviors is by using computational methods such as molecular dynamics. Molecular dynamics (MD) simulations, which were utilized in this study, have an advantage over experimental techniques by allowing for the study of the atomic scale conformational behavior that current experimental techniques may not be able to study, and also have the advantage of reducing the monetary cost and time for studying the mechanical properties of collagen fibrils. Computational models of molecular systems consist of large numbers of molecules, which results in the problem that the trajectories and thermodynamic properties of such systems are not easily modeled analytically. Molecular dynamics is a method for simulating large systems of particles through the use of numerical integration methods to solve the Newtonian equations of motion for the molecules using a specified interatomic potential, a set of ensemble conditions, and determining the molecular forces and trajectories. The ergodic

hypothesis states that for long periods of time, the probability that a system is in a particular microstate is the same for all microstates of the system. This allows for the prediction of thermodynamic properties of a whole system. There are, however, some limitations to MD simulations. The timescale of MD simulations should be comparable to the timescale of the actual physical process being simulated. The length of the MD simulation cannot also be too long, as its accuracy decreases as the length of time increases due to it being a numerical approximation. The timestep for the MD simulation must also be at least in the femtosecond range, as atoms are physically always vibrating at the femtosecond timescale and will not actually ever reach a minimum energy state. For the models in this investigation, the MD simulation time was approximately 6 ns for each MD simulation, with a timestep of 1 fs.

2.2 CHARMM Interatomic Potential

All the molecular dynamics models in this study were given periodic boundary conditions, which allowed for the modeling of larger conformations of collagen fibrils comparable to scales larger than that of a single short fibril. The CHARMM22 (Chemistry at HARvard Macromolecular Mechanics version 22) force field was used to describe the interactions between atoms in the fibril models [50]. This force field was selected because it has been optimized for protein MD simulations by adjusting parameters in order to compare MD simulations using the CHARMM22 force field to experimental data from techniques such as gas-phase geometries obtained from microwave and electron diffraction studies, vibrational spectra from gas-phase infrared and Raman spectroscopy, energy surface ab initio calculations, dipole moments, heats and energies of vaporization, solvation and sublimation properties, molecular volumes, crystal pressure and structure results from x-ray diffraction and spectroscopy, and mass spectrometry. The total bond energy between atoms in the CHARMM force field are described by Equation 2.1.1 [50].

$$\begin{aligned}
U(\vec{r}) = & \sum_{bonds} K_b(b - b_o)^2 + \sum_{UB} K_{UB}(S - S_o)^2 + \sum_{angles} K_\theta(\theta - \theta_o)^2 \\
& + \sum_{dihedrals} K_\chi(1 + \cos(n\chi - \delta)) + \sum_{impropers} K_{imp}(\varphi - \varphi_o)^2 \\
& + \sum_{nonbonded} \varepsilon \left[\left(\frac{R_{min_{ij}}}{r_{ij}} \right)^{12} - \left(\frac{R_{min_{ij}}}{r_{ij}} \right)^6 \right] + \frac{q_i q_j}{\varepsilon_1 r_{ij}}
\end{aligned} \tag{Equation 2.1.1}$$

For the bond term, K_b is the bond stretch force constant, and b is the bond length while b_o is the equilibrium bond length. For the Urey-Bradley term, K_{UB} is the Urey-Bradley force constant, and S is the Urey-Bradley 1,3 distance while S_o is the equilibrium Urey-Bradley 1,3 distance. For the angles term, K_θ is the bond angle force constant, and θ is the bond angle while θ_o is the equilibrium bond angle. For the dihedrals term, K_χ is the bond dihedral force constant, where χ is the bond dihedral angle while χ_o is the equilibrium bond dihedral angle. For the improper term, K_{imp} is the bond torsion force constant, and φ is the bond torsion angle while φ_o is the equilibrium bond torsion angle. Finally, the first term in the nonbonded interaction summation is the van der Waal's interaction represented by the 6, 12 Lennard-Jones potential where ε is the energy well depth, and r_{ij} is the distance between the two atoms and R_{min} is the equilibrium distance between atoms for a nonbonded Lennard-Jones interaction. The second term in the nonbonded interaction summation is the atomic electrostatic interaction where q_i is the partial atomic charge of the first atom, q_j is the partial atomic charge of the second atom, ε_1 is the effective dielectric constant, and r_{ij} is the distance between the two atoms. The Lennard-Jones interactions between different atom types for the CHARMM force field are calculated from the Lorentz-Berthelot combining rules, while all other cross-atom type interactions are explicitly listed in the CHARMM force field.

2.3 Fibril Models of Varying Mineral and Water Content

The model for the fibrils in this study were utilized from that determined in previous work by A. Gautieri et al. developed using homology modeling of type I collagen in the 3HR2 Protein Data bank

conformational structure [12, 28], which was determined from x-ray diffraction crystallographic analyses of brown rat collagen, while the collagen amino acid sequences are taken from the PubMed entry number NP_000079 for α_1 chains and NP_000080 for the α_2 chains. The unit cell for this model is triclinic [28, 29] with parameters of $a \approx 40.0 \text{ \AA}$, $b \approx 27.0 \text{ \AA}$, $c \approx 678 \text{ \AA}$, $\alpha \approx 89.2^\circ$, $\beta \approx 94.6^\circ$, and $\gamma \approx 105.6^\circ$. The collagen fibrils were mineralized at the three degrees of mineralization previously mentioned in Section 1.2: 0 wt%, 20 wt%, and 40 wt%. These degrees of mineralization were chosen in order to model only intrafibrillar mineralization, which was the goal of this study, without including extrafibrillar mineralization. The method of mineralization for the models was performed in a previous study using a Monte Carlo approach that was then validated by comparison to experimental studies that utilized cryogenic transmission electron microscopy, and low-dose selected-area electron diffraction [13, 30]. While substitution of the *OH* group in hydroxyapatite can result in the formation of other types of apatite in bone, as discussed in Section 1.1, this study utilized hydroxyapatite as the sole mineral apatite in order to model nascent bone, whose mineral phase is primarily composed of hydroxyapatite.

For each of the three degrees of mineralization, the fibrils were then hydrated with the 3-site TIP3P water model used by the CHARMM force field at approximately 0 wt%, 2 wt%, and 4 wt% water using the solvation plugin in VMD. Weight percentage was determined by multiplying the number of known water particles by the molecular weight of one water particle, which was determined from the Periodic Table of Elements, and dividing it by the total molecular weight of the fibril model. An amount of hydration between 0 wt% and 10 wt% water was chosen, since studies have found that healthy bone is composed of approximately 10 wt% water, as discussed in Section 1.1. For the mineralized fibril tensile and compressive tests of this study, there were then nine total models, which can be seen in Figure 2.2.1. Figure 2.2.1 (c) shows the fibril gap and overlap regions, as well as the model unit cell, whose length along the *x*-axis corresponds to the *D*-period length of 67 nm.

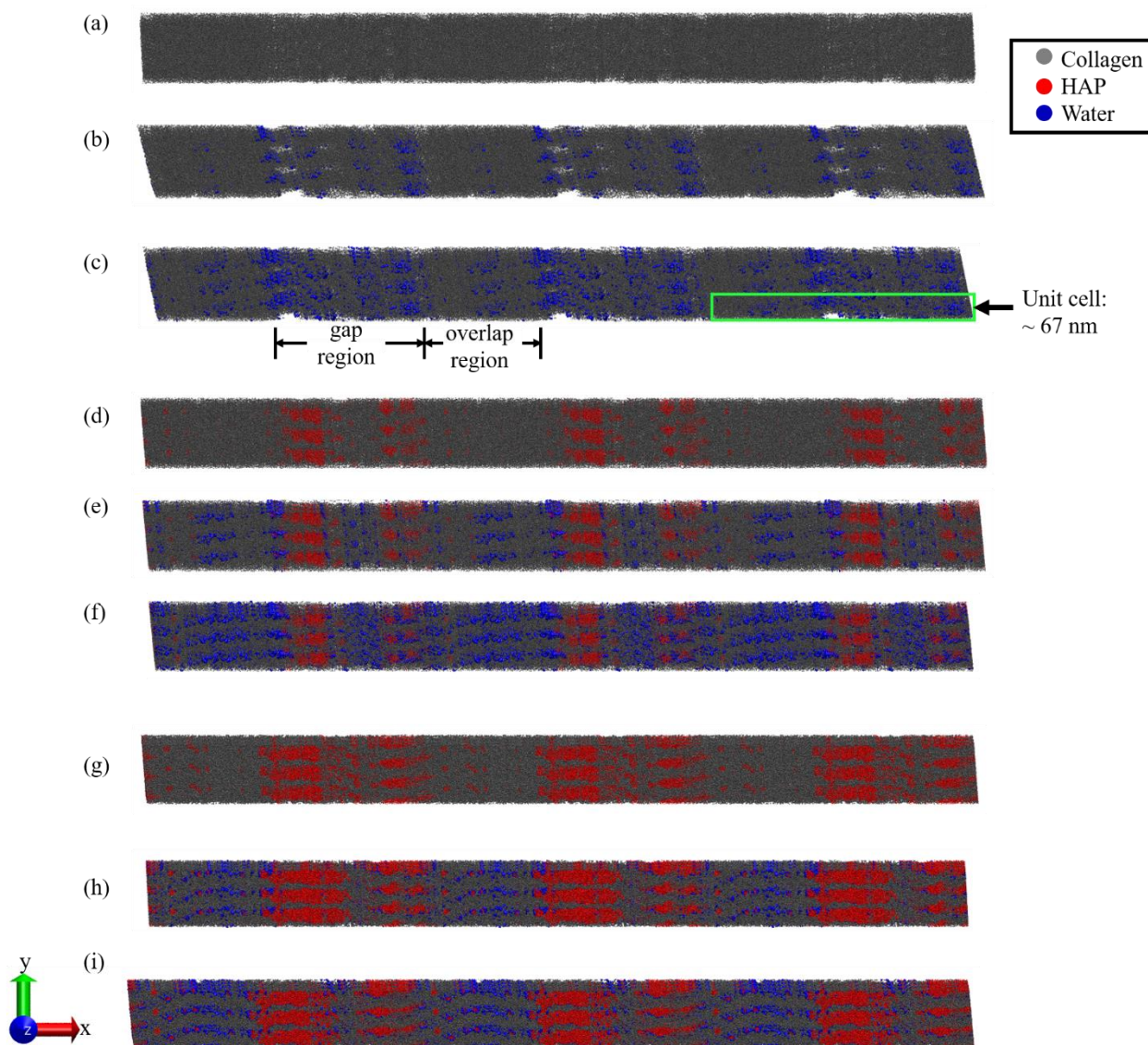


Figure 2.2.1 Collagen fibrils with varying mineral and water contents of (a) 0 wt% mineral and 0 wt% water, along with visualization of the unit cell (b) 0 wt% mineral and 1.2 wt% water, (c) 0 wt% mineral and 3.2 wt% water, (d) 20 wt% mineral and 0 wt% water, (e) 20 wt% mineral and 1.4 wt% water, (f) 20 wt% mineral and 4.2 wt% water (g) 40 wt% mineral and 0 wt% water, (h) 40 wt% mineral and 2.2 wt% water, (i) 40 wt% mineral and 3.3 wt% water. The grey atoms are type I collagen, apatite crystals are red color, and the blue color represents water molecules. Water contents are approximated as 0 wt%, ~2 wt%, and ~4 wt%.

The charmm2lammps tool was used to convert the fibril psf (protein structure file) and pdb (protein data bank) files into a LAMMPS data file utilizing the extended CHARMM force field. LAMMPS (Large-scale Atomic/Molecular Massively Parallel Simulator) is an open-source molecular dynamics program distributed by Sandia National Laboratories [51]. LAMMPS was chosen due to its common

use in the field of molecular dynamics research, its compatibility with a large number of interatomic potentials, such as CHARMM, and its flexibility in the functionality of the molecular dynamics simulation being run.

2.4 Tensile and Compressive Tests and Analysis of Deformation Mechanisms

Using MD as implemented in LAMMPS, a known tensile or compressive stress was applied to the fibril model unit cells. For the tensile tests, stresses of 1 atm, 5 MPa, 8 MPa, and 20 MPa were applied to the models in order to study the mechanical behavior of the fibrils at low initial stresses. For the compressive tests, stresses of 1 atm, 20 MPa, 60 MPa, and 100 MPa, were used in order to study the mechanical behavior of the fibrils at higher stress states, and in order to compare the results to previous studies. The periodic models were equilibrated in an *NPT* ensemble at a temperature of 300 K. The models were minimized and then equilibrated for approximately six nanoseconds in order to simulate a quasi-static stress state, since this study did not look into the effects of the rate of applied stress on the mechanical behavior of collagen fibrils. Equilibration of the models was confirmed when the slope of the root-mean-square distance between atoms in the system approached zero for several nanoseconds, which was determined to be approximately six nanoseconds. The strain of the models was then calculated using Equation 2.3.1 where ε is the linear strain, L is the equilibrium unit cell length of the fibril model in the stressed state, and L_o is the equilibrium unit cell length of the fibril model when subject to only 1 atm of pressure in all three orthogonal directions (x , y , z).

$$\varepsilon = \frac{(L-L_o)}{L_o} \quad (\text{Equation 2.3.1})$$

The stress was then plotted versus the strain, and a Young's modulus for the model was determined by Equation 2.3.2 where E is the Young's modulus, σ is the normal stress, and ε is the linear strain.

$$E = \frac{\partial \sigma}{\partial \varepsilon} \quad (\text{Equation 2.3.2})$$

The Young's modulus was then plotted versus the water content for all the models. An analysis of the fibril models' deformation mechanisms was done by plotting the gap/overlap ratio versus applied stress, where the gap/overlap ratio was the length of fibril gap region divided by the length of the fibril overlap region. The gap and overlap region lengths were determined by the distance between the fibril terminal amino acid residues, which correspond to the ends of the gap and overlap regions. A visual of this was shown in Figure 1.1.2.

2.5 Collagen Fibril and Carbon Nanotube Composites

As discussed in Section 1.1, studies have found CNTs to be a viable biocompatible constituent to strengthen bone scaffolds. This study looked at how CNTs of 10 nm, 20 nm, and 30 nm length in non-mineralized collagen fibrils with 43 wt% hydration affected the conformation, deformation mechanism, and mechanical behavior of the fibrils at compressive stresses of 1 atm, 20 MPa, 60 MPa, and 100 MPa, along the fibril length. The fibril/CNT composite models were hydrated at 43 wt% in order to model a hydrated environment, and compare to the analysis of a fully hydrated fibril determined in a previous study [52]. The composites were created by first creating a CNT model using the nanotube builder tool in VMD. The dimensions of the CNTs were determined based on previous studies of CNTs. An armchair CNT was chosen for this study in order to compare to other studies of CNTs (cited in Chapter 3) that used armchair CNTs. Experimental studies of CNTs found they were able to fabricate consistently CNTs of length 20-80 nm [53], and another study of bone scaffold composites containing CNTs found that CNTs on the order of 20 nm length are more eliminable by the human body, and induce a smaller immune response than larger CNTs [54]. Consistent fabrication of 10 nm long CNTs has also been shown to be possible [55, 56]. For this reason, lengths of 10 nm, 20 nm, and 30 nm was chosen for the CNTs, which also allows them to fit into the collagen fibril gap region more easily, which has a length of approximately 36 nm. The weight fraction of the CNTs for the fibril model in which they were included was calculated to be 5 wt% for the 10 nm long CNTs, 10

wt% for the 20 nm long CNTs, and 15 wt% for the 30 nm long CNTs. A diameter of 1 nm was chosen for the CNTs, in order to eliminate the effect of encapsulation of collagen fibrils into the CNT, since the fibrils have a diameter of approximately 1.5 nm. The CNT diameter was validated by a study that experimentally observed CNTs of diameter 0.85-1.3 nm in collagen and CNT bone scaffold composites [37]. To obtain this CNT diameter, indices of (7,7) were used based on Equation 1.1.1.

The VMD nanotube builder creates the CNT using the CHARMM aromatic carbon (CA) atom type. This atom type for the CNT was validated by performing tensile and compressive tests on the CNT along its length axis, and comparing the Young's modulus values to experimental results for the Young's modulus of CNTs. For each test a known strain was applied to the nanotube, and for each strain step the stress along the CNT length outputted by LAMMPS was plotted versus the linear strain. For the compressive test, strain data was used up until the nanotube lost its linear structure, since the harmonic CHARMM potential does not model bond breaking between atoms. The slopes of the stress versus strain plots were used to determine a tensile and compressive Young's modulus value of the CNT model and compare it to the Young's modulus of CNTs determined by other experimental and computational studies cited in Chapter 3.

The nanotubes were then placed in the gap regions of the fibril using the structure merging tool in VMD. The reasoning for placing the CNTs in the fibril gap region comes from previous studies whose scanning electron microscope analysis of collagen and CNT bone scaffold composites determined that CNTs arrange themselves in the spaces between collagen molecules in fibrils, and primarily in the fibril gap regions [37, 57]. An analysis of the mechanical behavior and deformation mechanisms of the fibril and CNT composites was performed using the methods outlined in Section 2.3.

Chapter 3: Results

In Chapter 3, the results of the fibril tensile tests are presented in Section 3.1. In Section 3.2, the fibril compressive tests are presented and which differ from the results of the fibril tensile tests. In Section 3.3, the tensile and compressive tests of individual carbon nanotubes are presented in order to validate the carbon nanotube model used in this study. Lastly, Section 3.4 shows the compressive tests of fibril/CNT composites, and compares the mechanical behavior of the fibril/CNT composites in compression to the mechanical behavior of fibrils without CNTs in compression.

3.1 Fibril Tensile Tests

For the non-mineralized fibril model, Figure 3.1.1 (a) shows the direction of tensile load applied along the fibril lengths. From Figure 3.1.1 (b) it was observed that an increase in water content from 0 wt% to ~4 wt% resulted in an approximately 300% increase in strain for an applied tensile stress of 20 MPa. For the 20 wt% mineralization case, from Figure 3.1.1 (c) it was observed that an increase in water content from 0 wt% to ~4 wt% resulted in the stress vs. strain behavior becoming more nonlinear, although there was only a 25% increase in deformation at a tensile stress of 20 MPa. For the 40 wt% mineralized fibril case, the total strain was reduced compared to the 20 wt% mineralized fibril at the same tensile stresses. The increase in strain at a 20 MPa tensile stress for the 40 wt% mineralized fibril when comparing from a water content of 0 wt% to ~4 wt% was approximately 27%.

It was observed that an increase in the intrafibrillar mineral content had the effect of increasing the stiffness of the fibril, while hydration caused the modulus of the fibril to decrease, as seen in Figure 3.1.1 (b,c,d). The results also indicated that hydration caused the stress versus strain behavior of the fibril to become more nonlinear, which agrees with results determined by J. Samuel et al. [58]. It was noted, however, that the degree to which hydration reduced the modulus relative to the non-hydrated fibrils was decreased by the presence of HAP. The stress versus strain results for the collagen fibrils for a tensile stress test at varying mineral and water content are shown in Figure 3.1.1. The effect of

water content on collagen fibril mechanical properties was also in agreement with the results observed by M.R. Uhlig and R. Magerle [59], who also observed that an increase in fibril water content produced an increased nonlinear stress versus strain behavior.

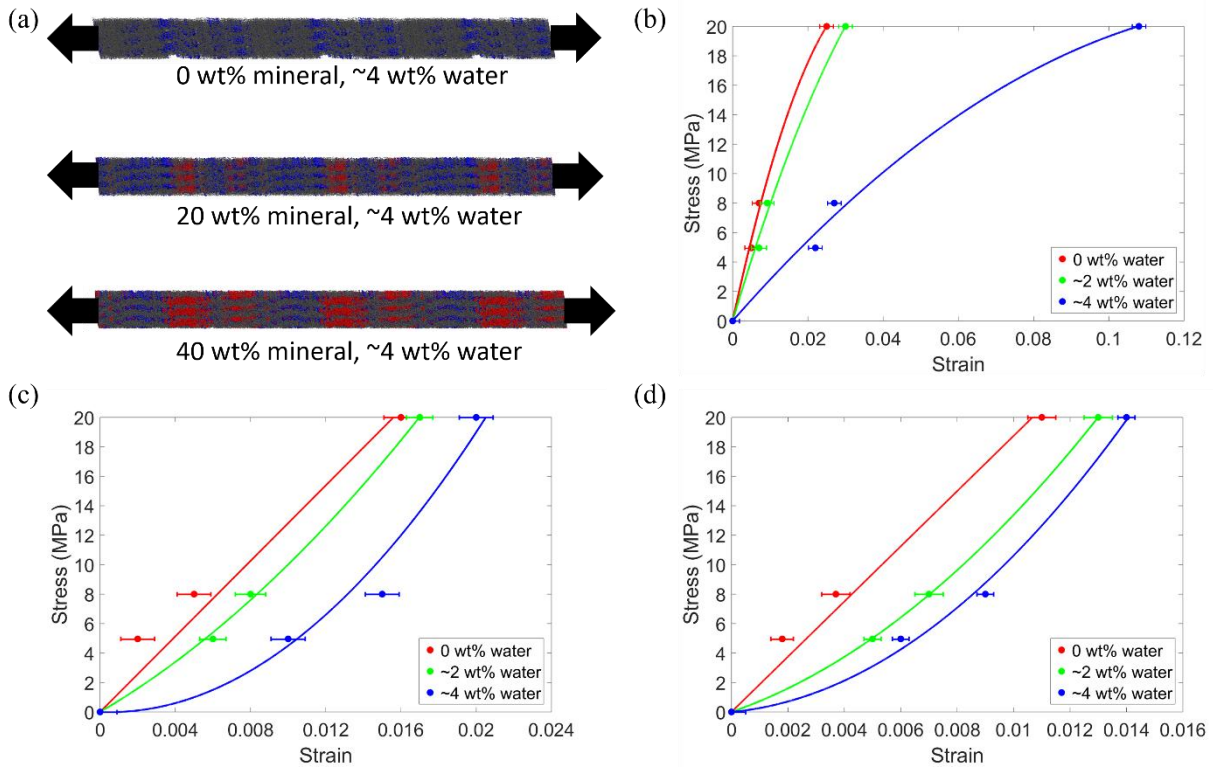


Figure 3.1.1 Tensile stress vs. strain of collagen fibrils. (a) The direction of tensile loading along the fibril lengths is shown for collagen fibrils with ~4 wt% water and three degrees of mineralization. Tensile stress vs. the linear strain of the fibrils is shown for models with mineral contents of (b) 0 wt%, (c) 20 wt%, (d) 40 wt%.

From Figure 3.1.2, it was observed that the Young's modulus of the 0 wt% mineralized fibrils with no water was approximately 1.2 GPa. An increase in water content from 0 wt% to ~2 wt% resulted in an approximately 33% decrease in Young's modulus. An increase in water content from ~2 wt% to ~4 wt% resulted in an approximately 26% decrease in Young's modulus. The decrease in the Young's modulus followed a linear trend as the fibril water content increased.

When the Young's modulus of the 20 wt% mineralized fibrils with no water in Figure 3.1.2 was studied, it was determined to be approximately 1.3 GPa. An increase in water content from 0 wt% to ~2 wt% resulted in an approximately 8% decrease in Young's modulus. An increase in water content

from 0 wt% to ~4 wt% resulted in an approximately 15% decrease in Young's modulus. The decrease in the Young's modulus also followed a linear trend as the fibril water content increased.

The Young's modulus of the 40 wt% mineralized fibrils with no water was approximately 1.9 GPa. An increase in water content from 0 wt% to ~2 wt% resulted in an approximately 10% decrease in Young's modulus, as is seen in Figure 3.1.2. An increase in water content from 0 wt% to ~4 wt% resulted in an approximately 15% decrease in Young's modulus. The decrease in the Young's modulus followed a linear trend as the fibril water content increased.

It was observed that the Young's modulus of the 40 wt% mineralized fibrils was close to double the Young's modulus of the non-mineralized fibrils, regardless of water content. For example, at ~2 wt% water for the non-mineralized fibril and ~2 wt% water for the 40 wt% mineralized fibril, the Young's modulus of the non-mineralized fibril in Figure 3.1.2 was 0.74 GPa which was a difference of about 117% compared to 1.61 GPa for the 40 wt% mineralized fibril. Also observed was a linear trend for the decrease in the Young's modulus as the water content increased for all three degrees of fibril mineralization.

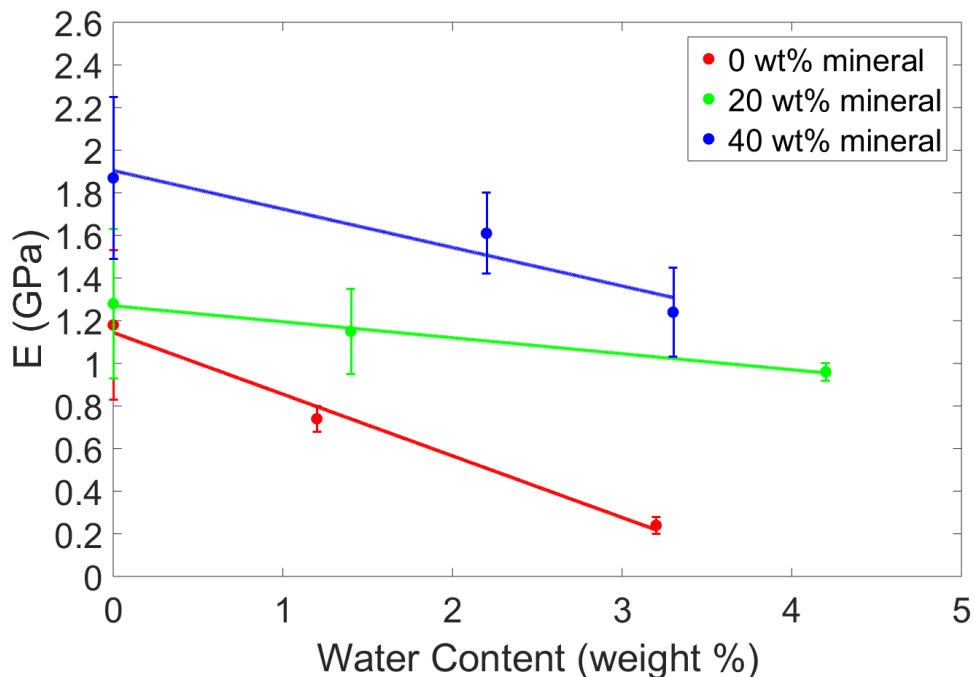


Figure 3.1.2 The tensile Young's modulus versus the fibril water content for fibrils of mineral contents of 0 wt%, 20 wt% and 40 wt%.

The result of the overall effect of hydration in reducing the Young's modulus of collagen fibrils was in agreement with other studies on collagen fibrils for mineralized and non-mineralized fibrils [10, 12, 52]. A direct comparison of the tensile Young's modulus values in this study from Figure 3.1.2 agrees with the results of other studies on the mechanical properties of collagen fibrils in Table 3.1.1. These studies used experimental and computational modeling methods to determine the Young's modulus of collagen fibrils. Some experimental techniques use x-ray diffraction [6], atomic force microscopy (AFM) [7, 60], and microelectromechanical system (MEMS) stretching [8, 9], while the computational methods used molecular dynamics (MD) [12, 13], and mathematical models [22]. Looking at the experimental values in Table 3.1.1, there is often a significant variation in the modulus values for fibrils with the same mineral and water contents. This is likely due to factors that were not considered in the experiments in Table 3.1.1 such as the amount of mineral substitution, the amount of mobile versus bound water, or the presence of collagen defects, all of which will change the fibril modulus. This highlights the importance of the MD study in this thesis, which controlled mineral and water content to determine the fibril modulus without the effects of mineral substitution, bound water, or collagen defects. Future work should look at how the addition of these variables affect the fibril modulus.

Table 3.1.1 Tensile Young's moduli obtained by other studies of collagen fibrils.

Young's modulus (GPa)	Mineral and water content	Method of testing
0.43	0% mineral – fully hydrated	X-ray diff.
0.2 to 0.8	0% mineral – fully hydrated	AFM
0.53	0% mineral – fully hydrated	MEMS Stretching
1.1 in the gap region	0% mineral – 0% water	MEMS Stretching
1.2 in the overlap region	0% mineral – 0% water	MEMS Stretching
0.3 to 1.2	0% mineral – fully hydrated	MD
1.8 to 2.25	0% mineral – 0% water	MD
0.5 to 1.1	0% mineral - 0% water	MD
1.3 to 2.7	20% mineral - 0% water	MD
1.5 to 2.8	40% mineral - 0% water	MD
2.4	32% to 61% mineral – 14% water	AFM
1.96	42% mineral – fully hydrated	Mathematical Model
2.4 ± 0.4	(46 ± 15)% mineral – 13% water	AFM/SEM

The Young's modulus values determined in this study were found to be in good agreement with the comparable values determined in other computational or experimental studies of collagen fibrils. The comparison of this study to the experimental modulus values in Table 3.1.1 is plotted in Figure 3.1.3. This study also compared the modulus values obtained in this MD study to the effective tensile modulus of a nanocomposite determined by the analytical model developed by Gao et al. [61] in Figure 3.1.3. The Gao model was developed to calculate the effective modulus of mineralized collagen fibrils based on the mineralized collagen fibril model developed by Jäger and Fratzl [62]. The formula for the effective modulus in the Gao model is given in Equation 3.1.1 [61]. \hat{E} is the effective modulus, ϕ is the mineral volume fraction, $G_{col.}$ is the collagen shear modulus of 0.03 GPa [13], ρ is the HAP mineral aspect ratio of 30 [13], and E_{HAP} is the elastic modulus of the HAP mineral of 100 GPa [13].

$$\frac{1}{\hat{E}} = \frac{4(1-\phi)}{G_{col.}\phi^2\rho^2} + \frac{1}{E_{HAP}\phi} \quad (\text{Equation 3.1.1})$$

At mineral volume fractions close to 0% in Figure 3.1.3, the modulus values in this study are higher than that determined by the Gao model. This is due to the mineral volume fraction term in Equation 3.1.1, which causes the effective modulus to approach zero as the mineral volume fraction approaches zero. At mineral volume fractions of 0%, it was found the results of this study agree most closely with the Gao model for fibrils with higher water content.

At mineral volume fractions of 50% in Figure 3.1.3, the modulus values from this study are lower than those determined by the Gao model. This is again due to the mineral volume fraction term in Equation 3.1.1. The maximum value possible for ϕ is when it is equal to unity. When ϕ approaches unity in Equation 3.1.1, the effective modulus becomes approximately the modulus of mineral, which neglects the full effects of collagen protein and water on the elastic modulus of highly mineralized fibrils. At mineral volume fractions of 50%, it was found the results of this study most closely

approximate the Gao model for fibrils with no water content. The modulus values in this study also agree most closely with the Gao model at intermediate intrafibrillar mineral volume fractions of 30%.

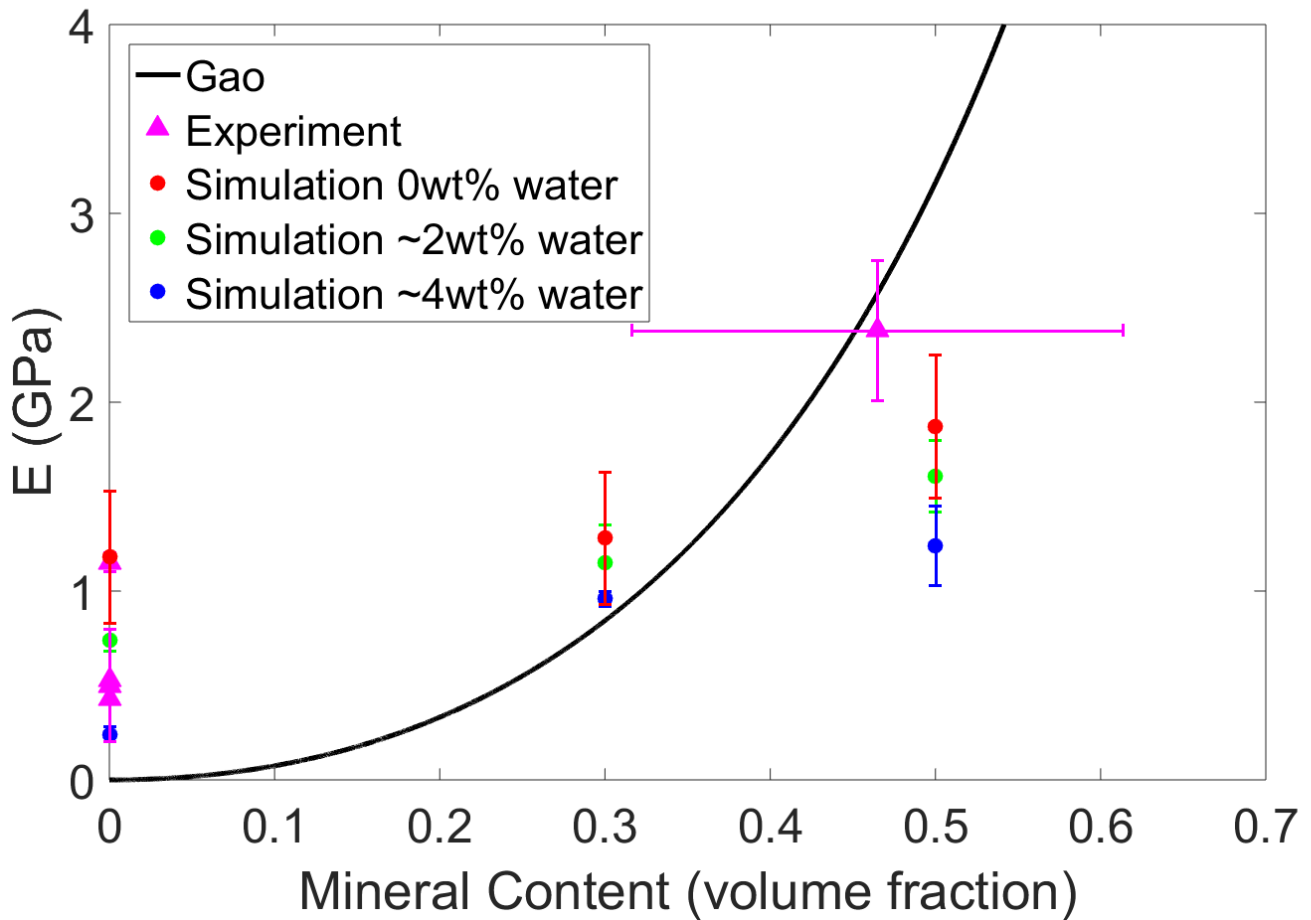


Figure 3.1.3 The tensile Young's modulus versus the fibril mineral content for modulus values determined in this study, from values from experiment, and the Gao model.

After analysis of the Young's modulus, this study investigated the deformation behavior of the fibril gap and overlap regions. The red and green points in Figure 3.1.4 are the terminal amino acid residues at opposite ends of each individual collagen molecule in the fibril. The distance between these terminal residues corresponded to the gap and overlap region lengths and was measured using VMD. The distance measured was used to analyze the linear deformation behavior for the gap and overlap regions for a tensile stress applied along the fibril length. The gap/overlap length ratio was used to analyze how the gap and overlap regions deformed relative to one another.

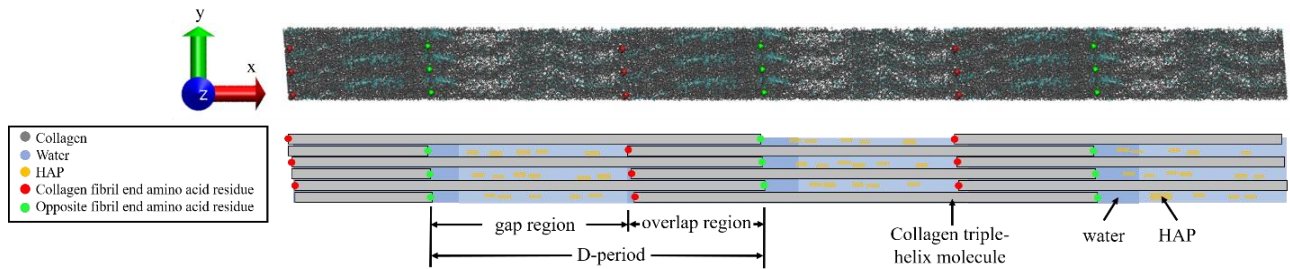


Figure 3.1.4 Fibril gap and overlap regions visualized in a schematic. The fibril is visualized atomically using VMD (top), and by a schematic (bottom).

The deformation behavior of the gap and overlap regions of the collagen fibril models are represented in Figure 3.1.5, Figure 3.1.6, and Figure 3.1.7, along with corresponding schematic diagrams for each model. The schematic diagrams shown in Figure 3.1.5, Figure 3.1.6, and Figure 3.1.7 also represent their respective collagen fibrils at an applied stress of 8 MPa, in order to better represent the effects of hydration and mineralization on deformation of the gap and overlap regions due to the applied stress. The gap length/overlap length ratios for the non-hydrated models in this study were in agreement with those determined by Nair et al. [13].

For the fibril cases of 0 wt% mineralization, it was observed that an initial increase in the fibril water content caused the gap length to deform more relative to the overlap region, corresponding to a decrease in gap/overlap ratio as stress increased as seen in Figure 3.1.5. At 2 wt% hydration, the water occupied voids in the gap regions and caused the overlap regions to contract. As the stress increased, the overlap regions began to unwind from contraction, and the gap/overlap ratio decreased.

At a hydration of 4 wt% for the non-mineralized fibril, the water still primarily occupied voids in the gap regions, but a slight amount of water occupied the overlap regions as well and prevented them from contracting. As the stress increased, the gap/overlap ratio remained approximately constant at 1.8, as seen in Figure 3.1.5. this demonstrated that as the stress increased, the gap and overlap region deformation was approximately the same when compared to one another.

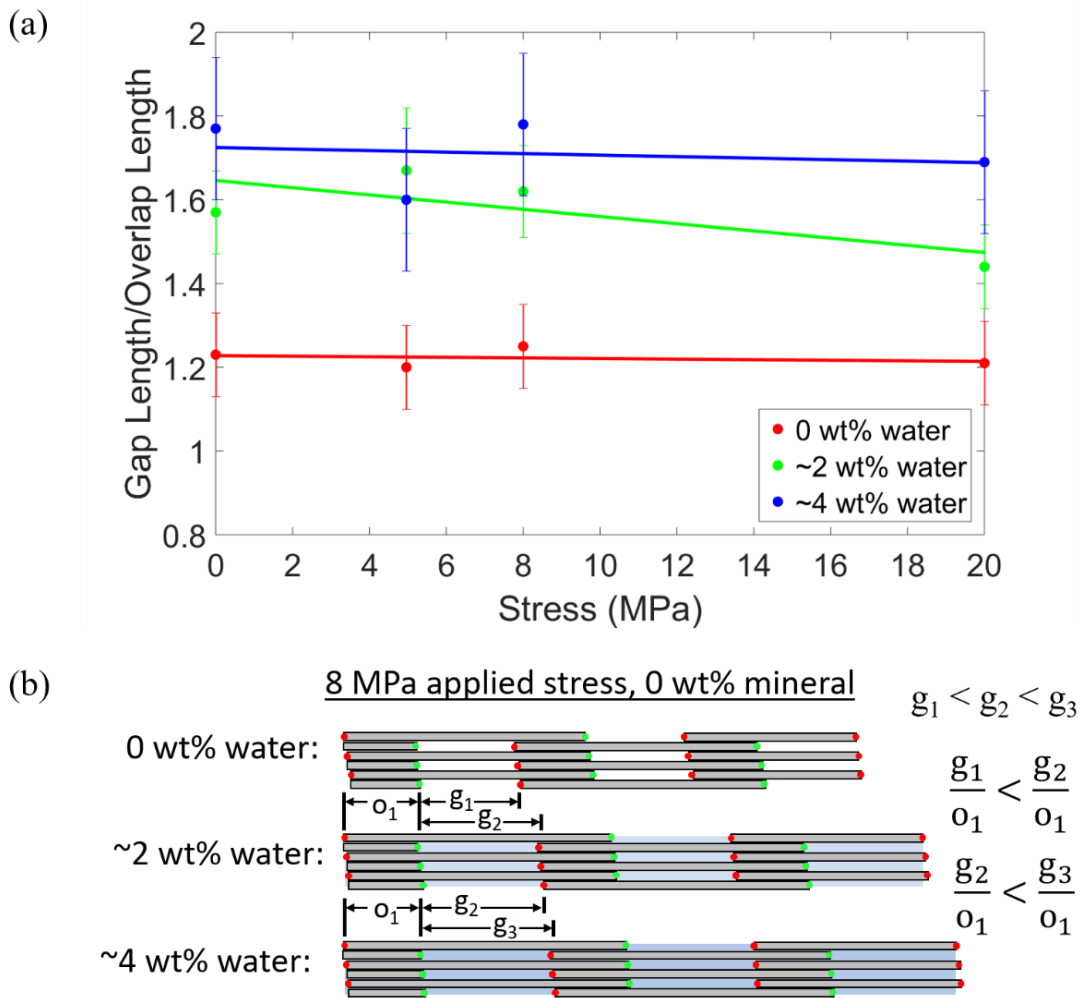


Figure 3.1.5 Gap/overlap ratio vs. tensile stress for non-mineralized fibrils (a). (b) A schematic of the non-mineralized fibrils under 8 MPa stress comparing the fibrils' gap and overlap regions at different water contents. The fibril overlap lengths are represented by the variable o with respective subscripts, while the fibril gap lengths are represented by the variable g with respective subscripts.

For the 20 wt% mineralized fibrils, the mineral was primarily in the gap region, and caused strain in the gap region to decrease by approximately 50%, even with changes in fibril water content from 0 wt%, to ~2 wt%, to ~4 wt%. The presence of mineral also reduced the effect of hydration on the gap/overlap ratio, where the addition of water did not cause as large of a magnitude change in the gap/overlap ratio in the 20 wt % mineralized fibrils as it did in the non-mineralized fibril, which was observed by a comparison of the 0 wt% mineral cases in Figure 3.1.5 (a) to the 20 wt% mineral cases in Figure 3.1.6 (a). The hydration of the 20 wt% mineralized fibrils to ~2 wt% water caused the

gap/overlap ratio of the fibril to initially decrease to approximately 1.15, but then the gap/overlap ratio increased to approximately 1.3 once the fibril water content increased to ~4 wt%. This was due to mineral that primarily occupied voids in the gap regions, which resulted in the gap regions having fewer spaces for the water to fill than the overlap regions. Because of this, it was found that the water was primarily occupied voids in the overlap region when the water content was ~2 wt%. This caused the overlap regions to expand and deform more relative to the overlap regions of the non-hydrated fibril as stress increased while the deformation of the gap regions remained relatively the same when comparing between the 0 wt% and ~2 wt% hydrated fibrils in Figure 3.1.6 (a).

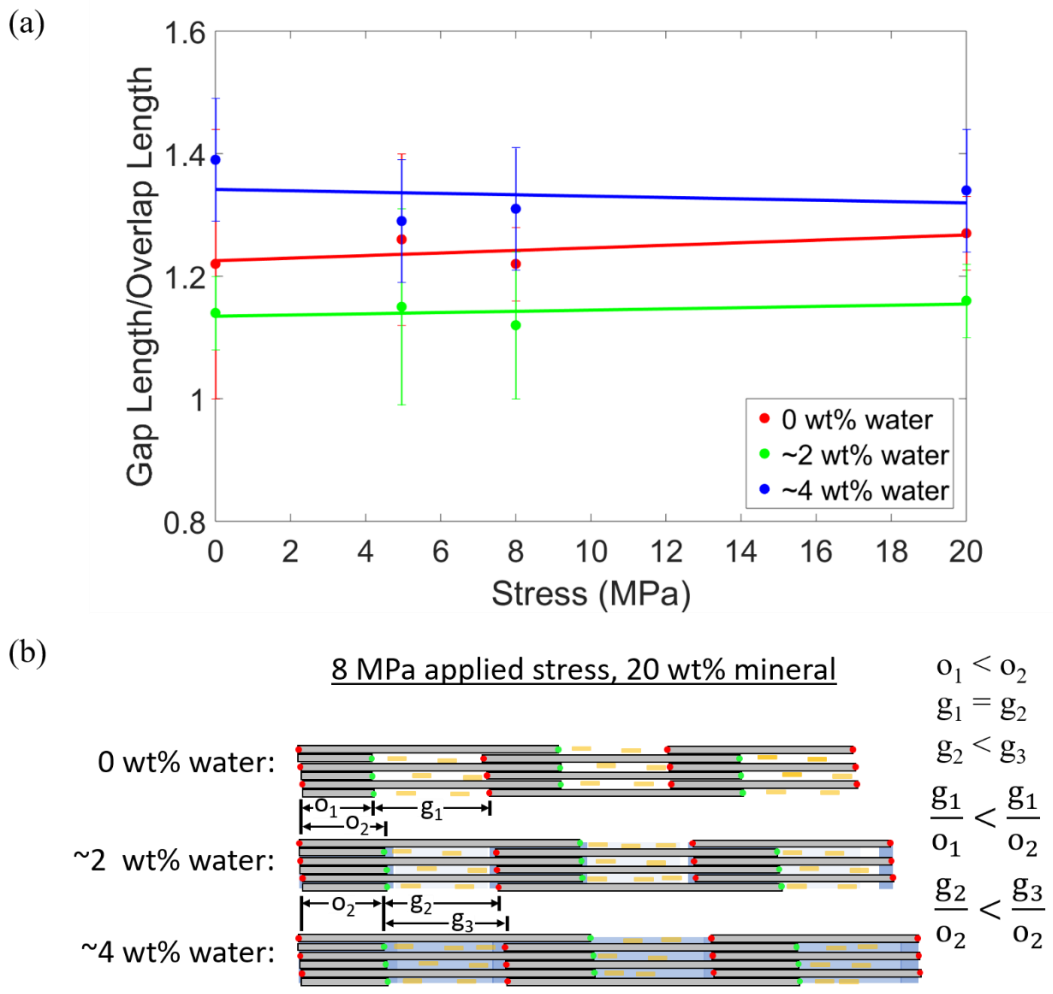


Figure 3.1.6 Gap/overlap ratio vs. tensile stress for 20% mineralized fibrils (a). (b) A schematic of the 20% mineralized fibrils shows a comparison between the fibrils' gap and overlap regions at different water contents. The fibril overlap lengths are represented by the variable o with respective subscripts, while the fibril gap lengths are represented by the variable g with respective subscripts.

However, as the water content increased to ~4 wt% in Figure 3.1.6, it was found that the water occupied void spaces in both the gap and overlap regions, and the water became much more uniformly distributed throughout the fibril. This was observed from Figure 2.2.1 (e,f), where the more uniform distribution of water in the fibril caused the gap regions to also expand and deform more compared to the deformation of the gap regions of the non-hydrated fibril as more stress was applied. This caused an increase in the gap/overlap ratio, as seen in Figure 3.1.6 (a).

For the 40 wt% mineralized fibril, the hydration of the fibril caused the gap/overlap ratio of the fibril to increase from approximately 1.3 to 1.5, as shown in Figure 3.1.7 (a). This was because the larger amount of mineralization caused a degree of mineralization to also occur in the overlap regions, although the greatest amount of mineral in the fibril remained in the gap regions. The presence of mineral in both the gap and overlap regions caused the water to distribute itself uniformly throughout the fibril into the spaces in both the gap region and the overlap region. This caused the gap regions of the 40 wt% mineralized fibril to deform more compared to the deformation of the gap region of the non-hydrated fibril of 40 wt% mineral when both experienced the same applied stress. Since the water caused both the overlap region and the gap regions to begin to expand and deform more, the gap/overlap ratio increased.

At a water content of ~2 wt%, most of the void spaces in the fibril were already occupied by the water. As the water content of the 40 wt% mineralized fibril increased to ~4 wt%, the water occupied remaining void spaces in the fibril and the gap/overlap ratio increased as the fibril expanded, but by a small fraction as seen in Figure 3.1.7 (a). The reason the gap/overlap ratio increased during hydration was that the water caused the gap regions to expand more than overlap regions parallel to the fibril axis, since the mineral in the gap region prevented the gap region from expanding much perpendicular to the fibril length axis while the overlap regions were free to do so. This was evident when comparing the ~2 wt% water model to the ~4 wt% water model in Figure 3.1.7 (a), where there is a minimal

difference between their respective gap/overlap ratios. The small difference in the water distribution when comparing the ~2 wt% and ~4 wt% hydrated fibril with 40 wt% mineral was observed in Figure 2.2.1 (h,i).

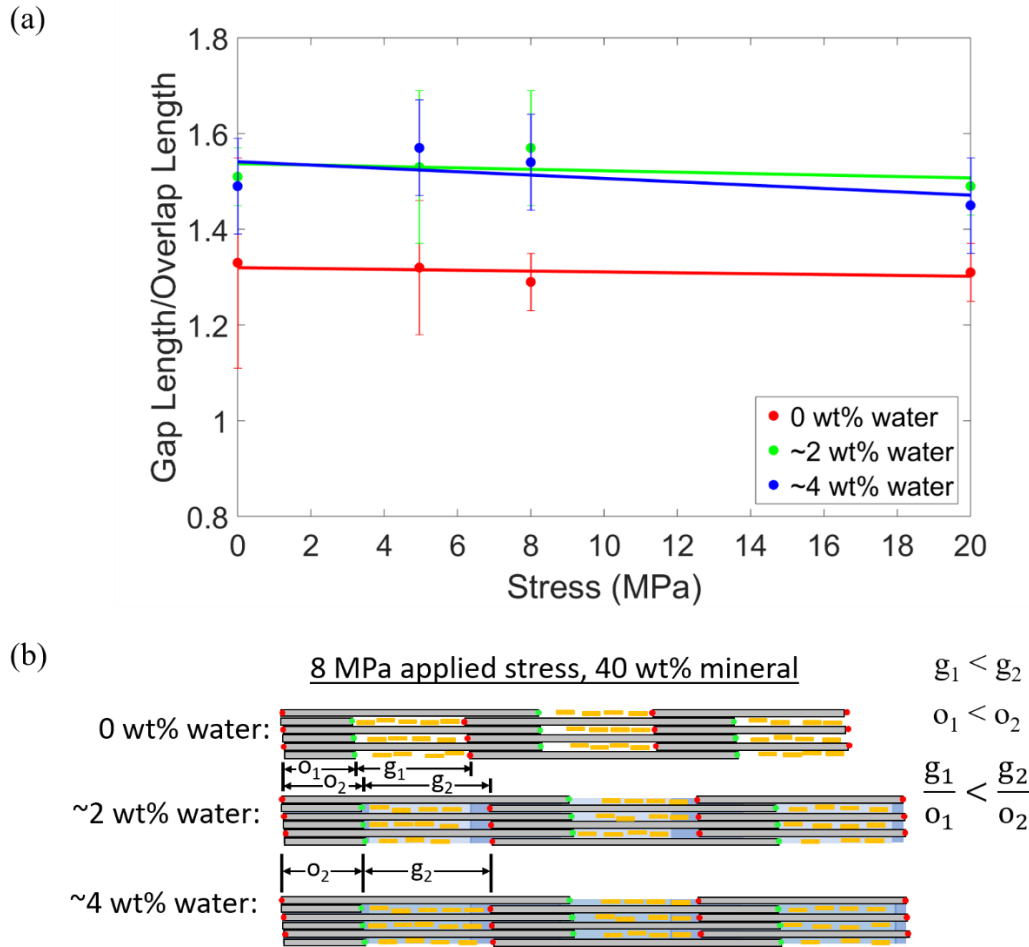


Figure 3.1.7 Gap/overlap ratio vs. tensile stress for 40% mineralized fibrils (a). (b) A schematic of the 40% mineralized fibrils shows a comparison between the fibrils' gap and overlap regions at different water contents. The fibril overlap lengths are represented by the variable o with respective subscripts, while the fibril gap lengths are represented by the variable g with respective subscripts.

It was also observed that as a higher tensile stress was applied to the fibril, the relation between the gap region deformation and the overlap region deformation remained approximately linear, regardless of the fibril water content. This can be seen in Figure 3.1.5 (a), Figure 3.1.6 (a), and Figure 3.1.7 (a). These results agreed with J. Samuel et al. [58], who observed a linear relation in bone between the mineral phase strain versus the collagen phase strain, which from the observations of this

study correspond primarily to the fibril gap regions and the fibril overlap regions, respectively. The results of this study, however, allowed for the use of the fibril gap/overlap length ratio to quantify the changes in the linear deformation relation between the mineral and collagen phases of protein when the fibril mineral content and water content simultaneously varied.

3.2 Fibril Compressive Tests

The compressive tests on non-mineralized and mineralized samples were next performed. Figure 3.2.1 (a) shows the direction of applied compressive stress along the fibril lengths for hydrated fibrils with mineral contents of 0 wt%, 20 wt%, and 40 wt%. From Figure 3.2.1 (b), it was found for non-mineralized fibrils under 60 MPa compressive stress that an increase in water content from ~2 wt% to ~4 wt% resulted in an approximately 31% increase in strain. From Figure 3.2.1 (c), it was found for 20 wt% mineralized fibrils under 60 MPa compressive stress that an increase in water content from ~2 wt% to ~4 wt% resulted in an approximately 9% increase in strain. Analysis of the results in Figure 3.2.1 (d) determined for 40 wt% mineralized fibrils under 60 MPa compressive stress that an increase in water content from ~2 wt% to ~4 wt% resulted in an approximately 120% increase in strain.

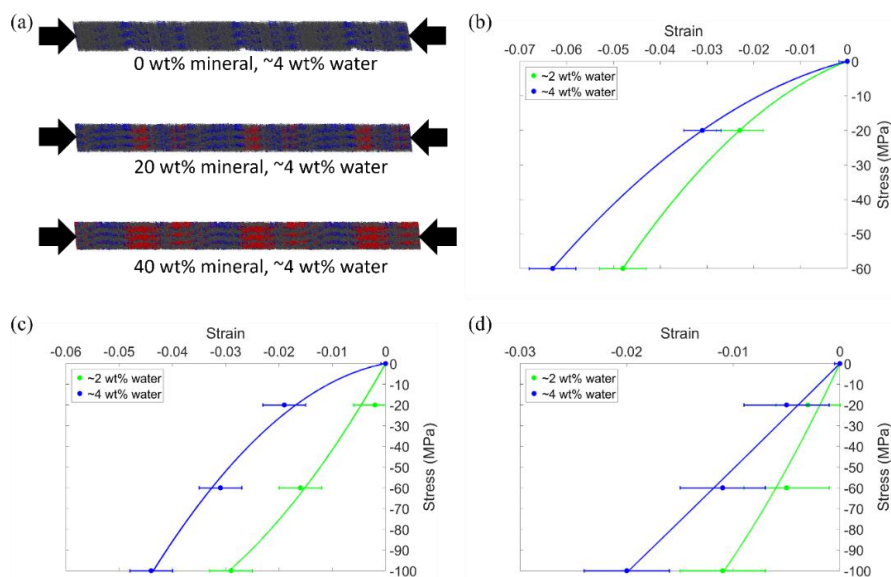


Figure 3.2.1 Compressive stress vs. strain of collagen fibrils. (a) Loading direction along the fibril length. Collagen is represented in gray, water in blue, and mineral in red. Stress vs. strain is shown for fibrils with mineral contents of (b) 0 wt%, (c) 20 wt%, and (d) 40 wt%.

It was observed in Figure 3.2.1 for all cases that as the fibril water content increased, the fibril strain increased. It was also found for all cases that as the fibril mineral content increased, the fibril strain decreased and the stress versus strain behavior became more linear. Analysis of fibrils in Figure 3.2.1 with ~2 wt% water and under 60 MPa tensile stress found that the increase in fibril mineral content from 0 wt% to 20 wt% resulted in an approximately 67% decrease in strain. A subsequent increase in fibril mineral content from 20 wt% to 40 wt% resulted in an approximately 69% decrease in strain.

The respective Young's modulus values for the models in Figure 3.2.1 were determined and plotted in Figure 3.2.2. The compressive modulus values determined by Nair et al. [52] were also represented in Figure 3.2.2 for comparison. For non-mineralized fibrils, it was found that an increase in water content from ~2 wt% to ~4 wt% resulted in a decrease in modulus from 1.22 GPa to 0.94 GPa, corresponding to an approximately 23% decrease in modulus. For 20 wt% mineralized fibrils, it was determined that an increase in water content from ~2 wt% to ~4 wt% resulted in a decrease in modulus from 3.3 GPa to 2.2 GPa, corresponding to an approximately 33% decrease in modulus. For 40 wt% mineralized fibrils, it was observed that an increase in water content from ~2 wt% to ~4 wt% resulted in a decrease in modulus from 9.35 GPa to 5.04 GPa, corresponding to an approximately 46% decrease in modulus.

Overall, it was observed that as the fibril water content increased, the modulus decreased. It was determined that as the fibril mineral content increased, a decrease in the fibril water content resulted in a larger decrease in fibril modulus. It was found that this was due to the water displaced from the gap regions to the overlap regions resulted in increased intermolecular sliding between overlapping collagen molecules in the overlap regions.

As the fibril mineral content increased, the modulus increased. However, it was observed that, in compression, the presence of water reduced the degree to which mineralization increased the modulus.

For example, for fibrils of ~2 wt% water, an increase in mineral content from 0 wt% to 40 wt% resulted in an increase in modulus from 1.22 GPa to 9.35 GPa. For fibrils of ~4 wt% water, an increase in mineral content from 0 wt% to 40 wt% resulted in an increase in modulus from 0.94 GPa to 5.04 GPa.

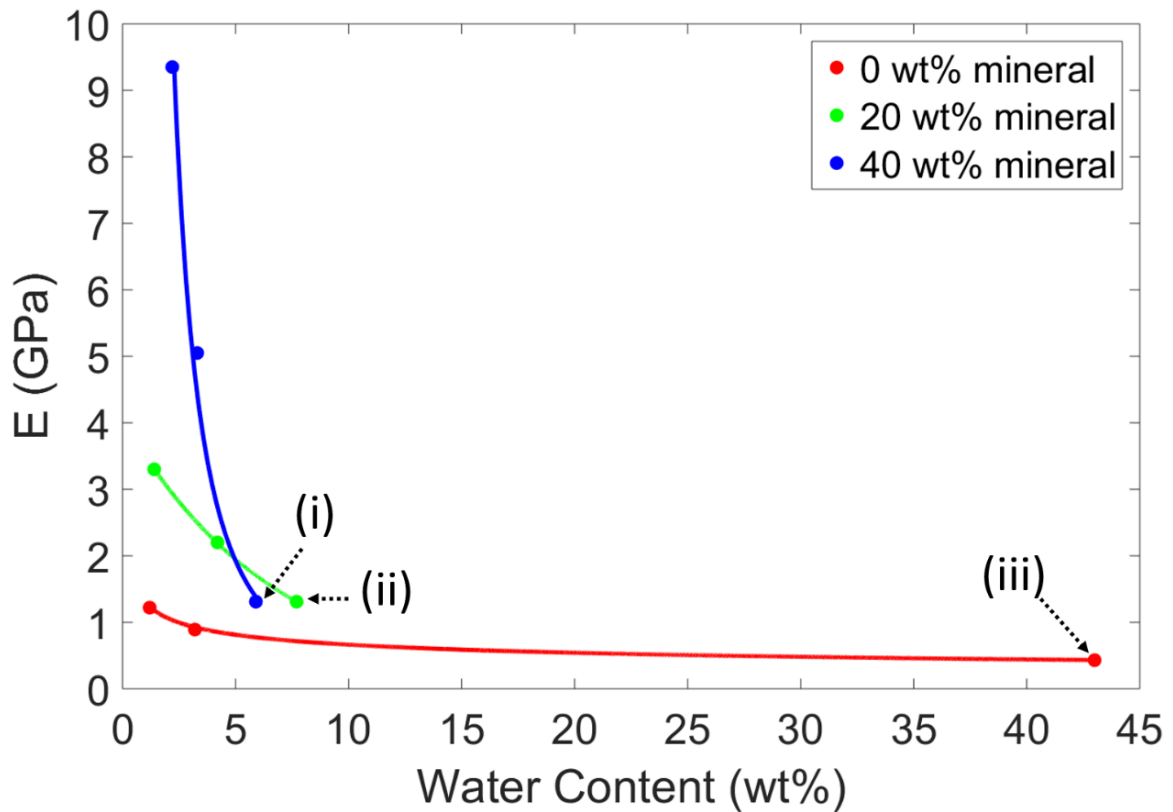


Figure 3.2.2 The compressive Young’s modulus versus fibril water content for fibrils with mineral contents of 0 wt%, 20 wt% and 40 wt%. The modulus values determined by Nair et al. [52] are also plotted as i, ii, and iii.

A comparison of fibril compressive modulus values from Figure 3.2.2 was made to the fibril compressive modulus values determined in other studies in Table 3.2.1 by experimental and computational methods. The other studies in Table 3.2.1 of highly mineralized fibrils that are dry or fully hydrated were compared to the 40 wt% mineral models in Figure 3.2.2 with ~2 wt% and ~6 wt% water, respectively. The other studies in Table 3.2.1 of non-mineralized fibrils that are dry or fully hydrated were compared to the 0 wt% mineral models in Figure 3.2.2 of ~2 wt% and 43 wt% water, respectively. It was found that the compressive modulus values for fibrils in this study were in good

agreement with the compared modulus values of the other studies in Table 3.2.1. The results of this study also gave insight into the modulus values of partially mineralized and partially hydrated fibrils, which is crucial to the study of bone, since bone mineral and water content do not abruptly decrease, but gradually decrease with age.

Table 3.2.1 Compressive Young's moduli obtained by other studies of collagen fibrils.

Young's modulus (GPa)	Mineral and water content	Method of testing
1.22 (this study)	0 wt% mineral, ~2 wt% water	MD
0.43 [52]	0 wt% mineral, 43 wt% water	MD
9.35 (this study)	40 wt% mineral, ~2 wt% water	MD
1.31 [52]	40 wt% mineral, 43 wt% water	MD
1.9 ± 0.5 [63]	0 wt% mineral, 0 wt% water	AFM nanoindentation
1.3 ± 0.1 [63]	0 wt% mineral, fully hydrated	AFM nanoindentation
1.26 ± 0.354 [64]	0 wt% mineral, 0 wt% water	AFM nanoindentation
0.03 ± 0.01 [64]	0 wt% mineral, fully hydrated	AFM nanoindentation
1.2 to 2.2 [9]	0 wt% mineral, 0 wt% water	AFM nanoindentation
13.87 ± 8.24 [65]	highly mineralized, 0 wt% water	AFM nanoindentation
0.003 ± 0.001 [65]	highly mineralized, fully hydrated	AFM nanoindentation
~11.4 [66]	highly mineralized, 0 wt% water	MD
~7.8 [66]	highly mineralized, fully hydrated	MD
6 to 10 [67]	60% mineral, slightly hydrated	Synchrotron x-ray scattering/backscattered electron imaging

The compressive modulus values of this study were in good agreement with values obtained in the other studies in Table 3.2.1. Looking at the experimental values in Table 3.2.1, there is often a significant variation in the compressive modulus values for fibrils with the same mineral and water

contents. Like experimental tensile tests of collagen fibrils, this variation in compressive modulus is likely due to factors that were not considered in the experiments in Table 3.2.1 such as the amount of mineral substitution, the amount of mobile versus bound water, or the presence of collagen defects, all of which will change the fibril modulus. This highlights the importance of the MD study in this thesis, which controlled the variables of mineral and water content to determine the fibril modulus without the effects of mineral substitution, bound water, or collagen defects. Future work should look at how the addition of these variables affect the fibril modulus.

Analysis was also done to compare the modulus values obtained in these MD studies to the effective compressive modulus of a nanocomposite determined by the Gao model [68] in compression. The Gao model parameters and governing equation remain the same as Equation 3.1.1. It was found that the MD simulation results for Young’s modulus in this investigation were in good agreement with the Gao model for effective modulus in Figure 3.2.3.

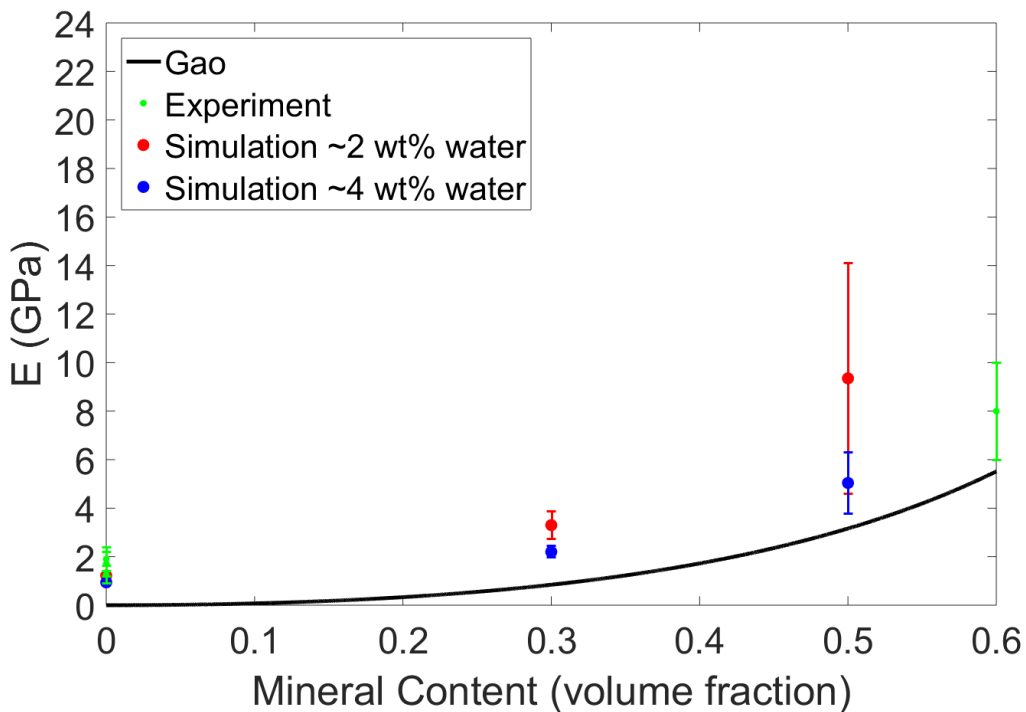


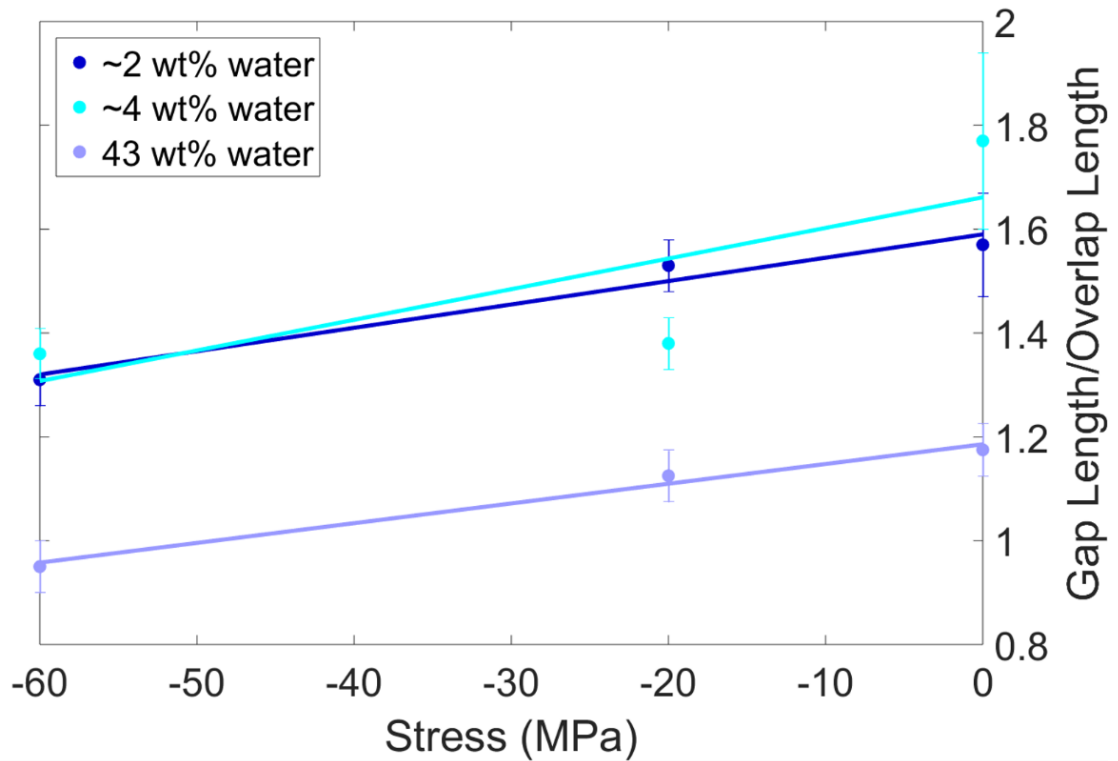
Figure 3.2.3 The compressive Young’s modulus vs. fibril mineral content. The MD simulation compressive modulus is plotted versus fibril mineral content for fibrils with water contents of 2 wt% (red) and 4 wt% (blue).

The results of the other studies in Table 3.2.1 are also plotted in Figure 3.2.3. As seen in Figure 3.2.3, the MD simulation Young's modulus results from this study agreed well with the Gao model for effective modulus for fibrils at 2 wt% and 4 wt% water, and follow a similar trend for the increase in modulus for an increase in mineral fraction. However, the fibrils with 4 wt% water agreed better with the Gao model than the fibrils with 2 wt% water. This was likely due to the collagen shear modulus, which should change to reflect the change in fibril water content. The MD simulation results follow a similar trend as the Gao model, but are slightly higher. As mentioned in Section 3.1, this is due to the fact that at low mineral volume fractions, the Gao model effective modulus reduces to zero, and does not take into account the modulus of the remaining collagen protein and water.

After analyzing the compressive modulus values of the fibrils, this study investigated the deformation mechanisms of the fibrils by analyzing the fibril gap/overlap ratio. For non-mineralized fibrils, it was observed that at an increase in water content from ~2 wt% to ~4 wt% resulted in an approximately 13% increase in the gap/overlap ratio as can be seen in Figure 3.2.4 (a). This was due to the fact that, at low water contents, the water primarily occupied voids in the gap regions. As the water content increased, it resulted in an expansion of the gap region lengths while the overlap region lengths remained approximately the same as is represented in the schematic in Figure 3.2.4 (b). This corresponded to an increase in the gap/overlap ratio.

As the fibril water content increased from ~4 wt% to 43 wt%, the water fully hydrated both the fibril gap regions and overlap regions. This caused the overlap regions to also expand due to the presence of water and the gap/overlap ratio decreased from 1.77 for ~4 wt% hydration to 1.2 for 43 wt% hydration as seen in Figure 3.2.4 (a). It was also observed that as compressive stress was applied to the non-mineralized fibrils, the gap/overlap ratio decreased. This demonstrated that the gap regions deformed more than the overlap regions under compressive stress. While the gap/overlap ratio decreased as stress increased, the decrease in the gap/overlap ratio remained approximately constant.

(a)



(b)

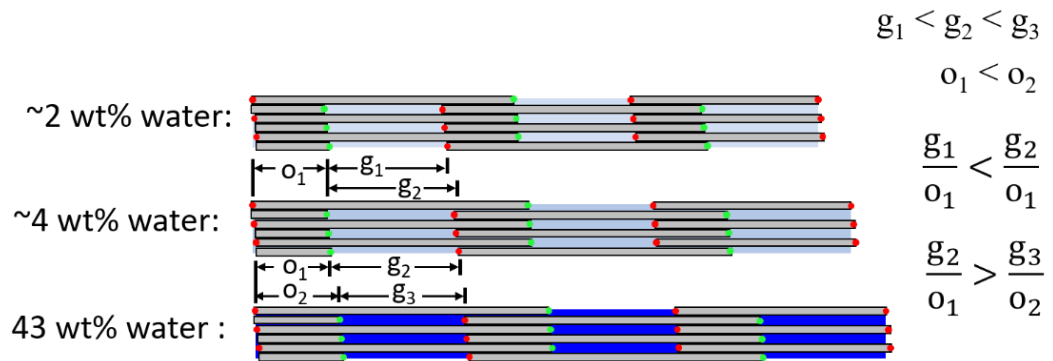


Figure 3.2.4 Gap/overlap ratio versus compressive stress for non-mineralized fibrils (a). (b) Schematics showing the length of the fibril gap and overlap regions under 1 atm pressure.

The gap region and overlap region deformation behavior for fibrils with 20 wt% mineral is observed in Figure 3.2.5. At a fibril water content of ~2 wt%, it was observed that the water was primarily located in the overlap regions due to the presence of mineral in the gap regions. The presence of water in the overlap regions increased intermolecular sliding and mineral in the gap regions resisted compression of the gap regions. This resulted in the overlap regions deforming more than the gap

regions and the gap/overlap ratio increased as the compressive stress increased.

As the fibril water content increased from ~2 wt% to ~4 wt%, the gap/overlap ratio at no applied stress increased by approximately 22%. This was because, at ~4 wt% water, the water distributed evenly throughout the whole fibril, and caused a slight expansion of the gap regions and resulted in a decrease in the initial gap/overlap ratio. As stress was applied to the fibril with ~4 wt% water, the gap/overlap ratio remained approximately constant. The results in Figure 3.2.5 were also in good agreement with a previous study by Nair et al., which is shown as the fibril with ~8 wt% water in Figure 3.2.5 [52].

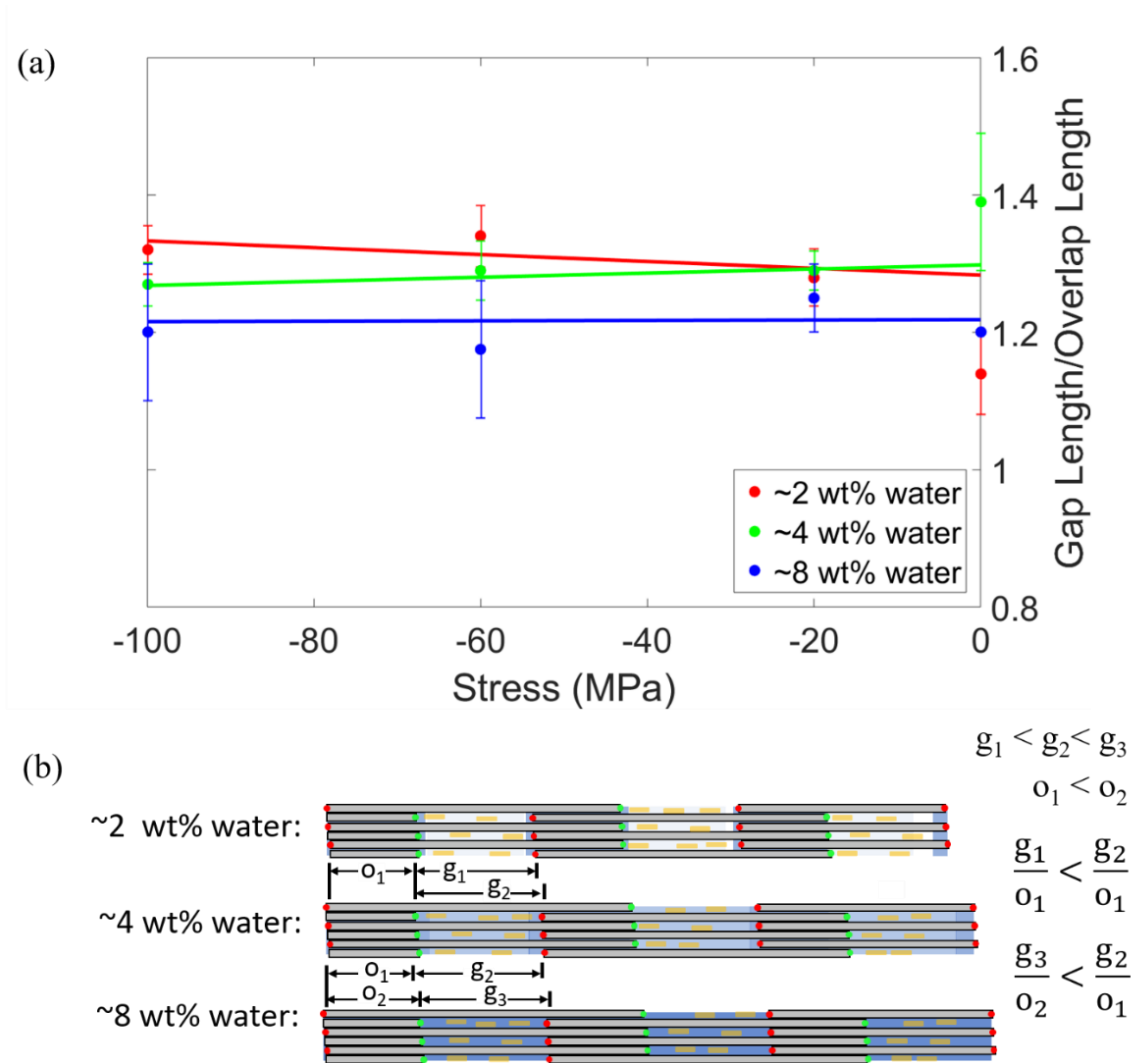


Figure 3.2.5 Gap/overlap ratio versus compressive stress for 20 wt% mineralized fibrils (a). (b) Schematics showing the deformation of the fibril gap and overlap regions.

As the water content increased from ~4 wt% to ~8 wt%, the gap/overlap ratio decreased in Figure 3.2.5, since the overlap region expanded due to the increase in hydration, but the mineral in the gap regions resisted expansion of the gap regions. This agreed with experimental results that determined that high fibril hydration resulted in a compressive pre-strain of the collagen fibril mineral phase, which was primarily located in the gap regions for the models in this investigation [58]. This study also found that an increase in fibril water content increased the *D*-period of the fibril, which is the combined length of the gap and overlap region. This also agreed with the results of the previously mentioned experiment [58], which also observed an increase in the *D*-period of mineralized fibrils as their water content increased. However, this study was able to also investigate the change in the gap and overlap regions lengths.

The gap/overlap ratio behavior under compressive stress for fibrils with 40 wt% mineral is presented in Figure 3.2.6. The results for this case for fibrils with ~2 wt% water and ~4 wt% water were in good agreement with the results from a previous study of a fibril with ~6 wt% water in [52], with a gap/overlap ratio at approximately 1.5. The results of that study for the fibril with ~6 wt% water are also shown in Figure 3.2.5 for comparison to the fibrils with ~2 wt% and ~4 wt% water in this study. It was observed that, even at water contents as low as ~2 wt%, the water distributed uniformly throughout the fibril. It was found for all degrees of hydration that as the water content increased, the gap/overlap ratio increased, because the water caused an expansion of the overlap regions while the presence of mineral in the gap regions resisted expansion of the gap regions. This was in agreement with previous experimental studies of mineralized collagen fibrils that observed compressive pre-strain in the mineral phase of the fibrils [58].

It was observed in Figure 3.2.6 that as the fibril water content increased from ~2 wt% to ~6 wt%, the magnitude of the slope of the gap/overlap ratio versus the applied stress increased. This was because an increase in the fibril water content caused a larger increase in the deformation of the

overlap regions than the deformation of the gap regions, since the increased water content in the overlap regions increased intermolecular sliding in the overlap regions, while mineral in the gap regions resisted the compression of the gap regions. This also agreed with previous experimental studies of mineralized collagen fibrils that observed an increase in the *D*-period length when the fibril water content increased [58], while this study also enabled the investigation of the change in gap and overlap region lengths.

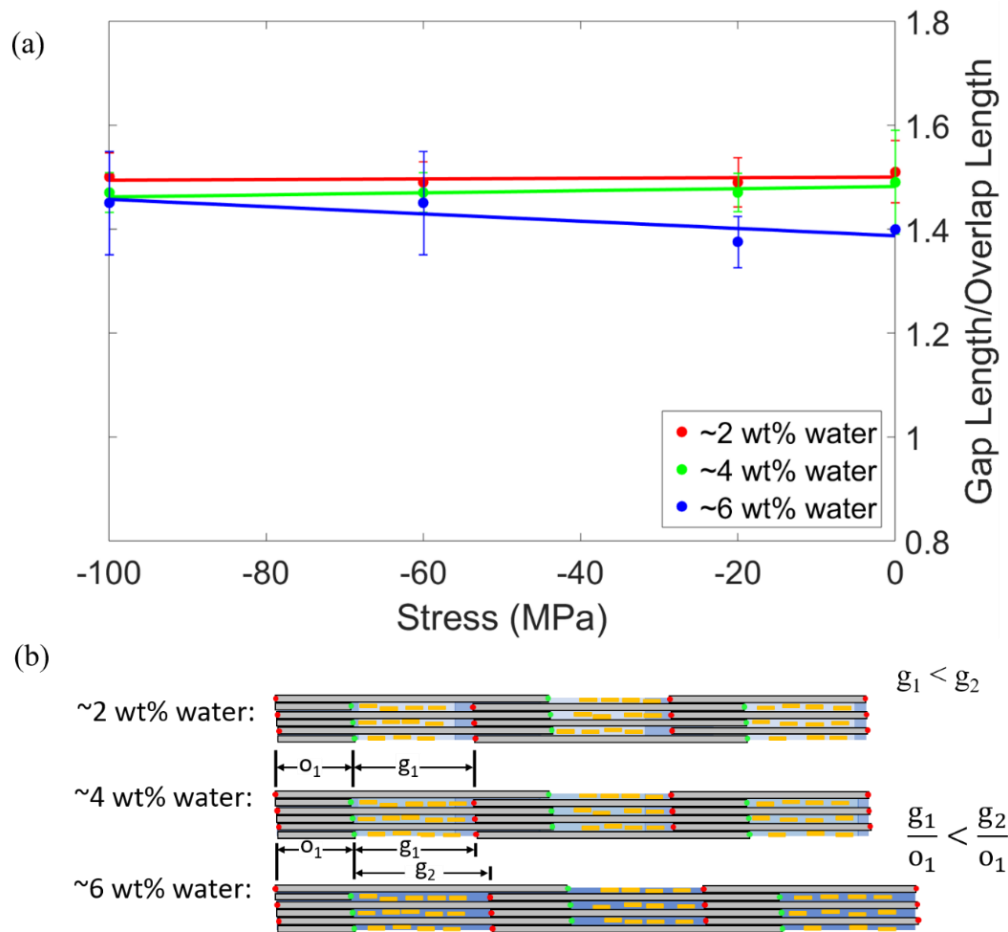


Figure 3.2.6 G/overlap ratio versus compressive stress for 40 wt% mineralized fibrils (a). (b) Schematics showing the fibril gap and overlap regions at 1 atm pressure.

The tensile and compressive tests on non-mineralized and mineralized samples show the different deformation behavior and change in Young's modulus as the loading changes. The next area of exploration was the use of CNTs as a substitute for mineral found in bone at the nanoscale to study the deformation behavior and quantify the mechanical properties.

3.3 Carbon Nanotube Tensile and Compressive Tests

A tensile test was performed along the length of a 20 nm long CNT with a 1 nm diameter and modeled with the *CA* atom type in the CHARMM potential; it was found that Young's modulus was approximately 1.051 TPa. Figure 3.3.1 (a) shows the direction of the application of the tensile load to the CNT, while Figure 3.3.1 (b) shows the results of the stress vs the strain of the CNT. The Young's modulus of the CNT was calculated as the slope of the linear fit of the stress vs the strain. A comparison to the CNT tensile modulus determined by computational and experimental methods is shown in Table 3.3.1. The CNT tensile modulus value determined in this study were in good agreement with that of the studies presented in Table 3.3.1, and validated the use in this study of the CHARMM *CA* atom type to model CNTs.

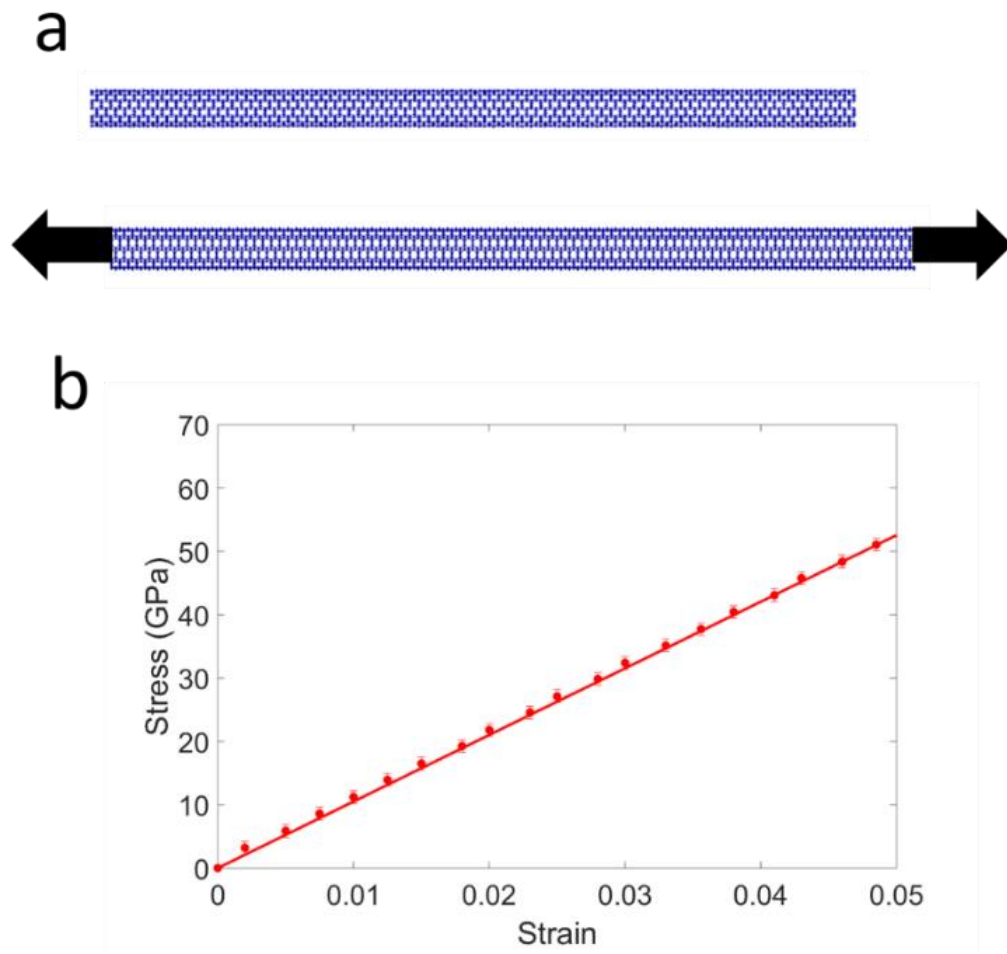


Figure 3.3.1 Tensile test of a carbon nanotube. The CNT is 20 nm long, and 1 nm diameter CNT (a). (b) the stress vs. strain for the CNT tensile test.

Table 3.3.1 Tensile Young's moduli of CNTs determined by other studies.

Study group	Method	Young's Modulus (TPa)
This study: tensile test	MD: CHARMM	1.051 ± 0.01
[69]	MD: AMBER	~ 1
[70]	Empirical force constant model	1
[71]	Born perturbation technique Lattice-dynamical model	1
[72]	Tight-binding formalism	1.24
[73]	AFM	1.31
[74]	TEM	Length = 23.4 nm, Diameter = 1.12 nm, $E=1.02 \pm 0.2$

While the CNT tensile test corroborated the model of the CNT used in this study, compression tests on CNTs were also performed in order to determine if the compression Young's modulus of the CNTs changed based on a change in CNT length, since the CNTs utilized in this study varied in length and were under compressive stress. Figure 3.3.2 shows the results of the compressive tests of the 10 nm, 20 nm, and 30 nm length CNTs used in this study.

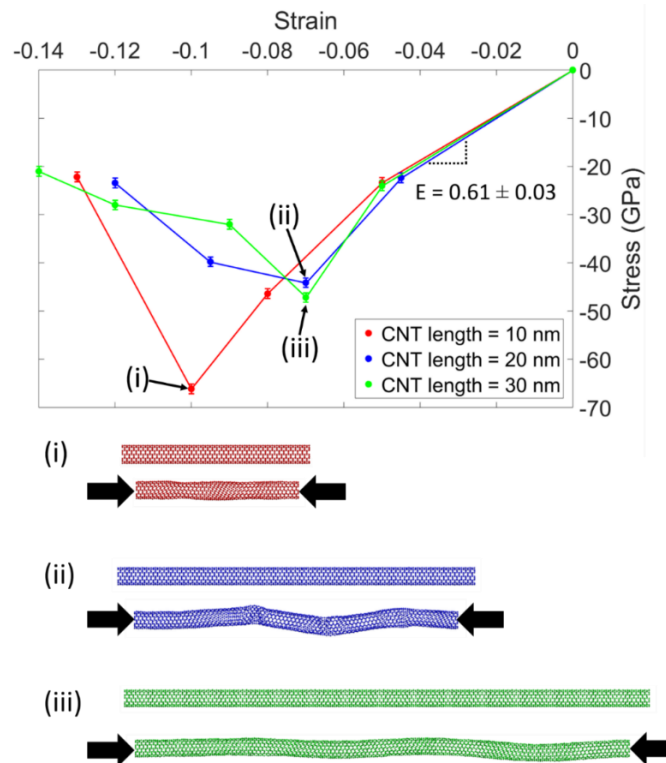


Figure 3.3.2 Compressive stress versus strain of carbon nanotubes. The CNTs are 1 nm in diameter and of varying length. The conformation of the nanotubes before structural failure while under compressive stress is shown in (i, ii, iii).

While the weight percent of CNTs in the fibril/CNT composite models changed due to the difference in CNT lengths, Figure 3.3.2 shows that, at compressive stresses lower than 20 GPa, the Young's modulus was approximately 610 MPa regardless of the CNT length. This modulus was chosen for all the CNTs used in this study, since the maximum stress applied to the fibril/CNT composites was 60 MPa. This also meant that investigating how a change in CNT modulus due to CNT length changed the mechanical behavior of the fibril/CNT composites did not have to be considered in this study, since the change in the CNT modulus due to a change in CNT length was negligible.

3.4 Fibrils with CNTs Compressive Tests

Figure 3.4.1 shows the conformation of the fibril models with CNTs. As mentioned in Section 2.4, the CNTs were placed into the gap region. The 10 nm long CNTs corresponded to 5 wt% of the total fibril, the 20 nm long CNTs corresponded to 10 wt% of the total fibril, and the 30 nm long CNTs corresponded to 15 wt% of the total fibril. It was observed that as the CNT concentration increased, the overall fibril length expands.

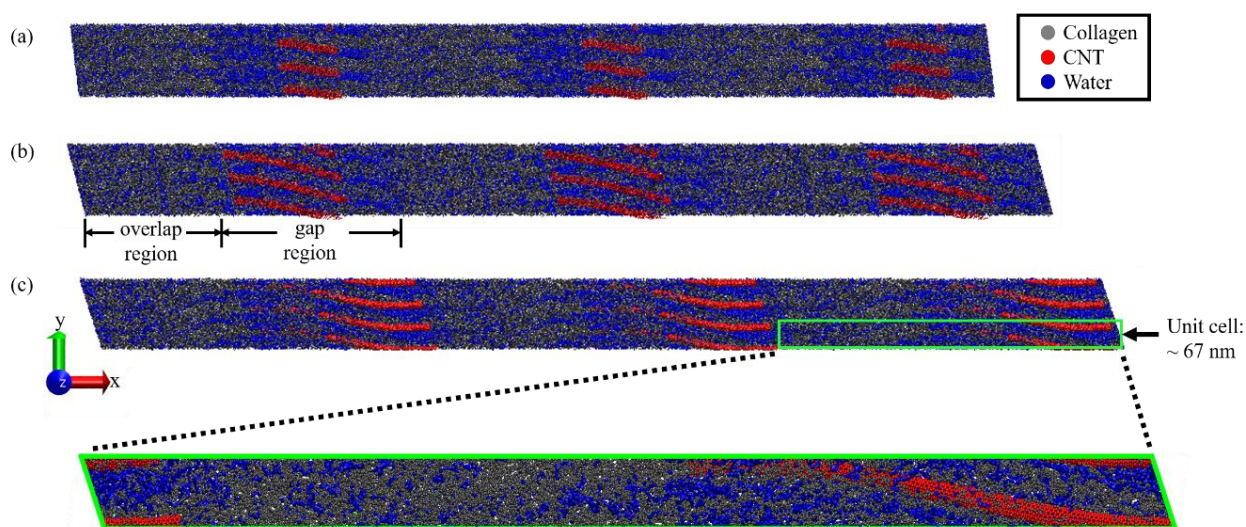


Figure 3.4.1 Collagen fibrils with CNTs in the gap regions. Atomistic representations are shown of collagen fibrils with 43 wt% water and (a) 5 wt% CNTs, (b) 10 wt% CNTs, and (c) 15 wt% CNTs at 1 atm pressure in all directions. In panel (c) an enlarged view of the unit cell is shown.

From Figure 3.4.2 (b), it was found for non-mineralized fibrils with 43 wt% water and under 60 MPa compressive stress, that an increase in CNT content from 5 wt% to 15 wt% resulted in an approximately 43% decrease in strain. It was also observed that, while the fibrils with CNTs had a larger amount of water content compared to the fibrils without CNTs, the addition of CNTs to the fibril resulted in a decrease in fibril strain compared to the fibrils with no CNTs and low water contents of ~2 wt% and ~4 wt%. The maximum strain at 60 MPa stress for the fibrils with CNTs in Figure 3.4.2 (a) was approximately 0.03, which was comparable to the maximum strain of approximately 0.03 at 60 MPa stress for the fibrils with 20 wt% mineral in Figure 3.4.2 (c). The fibrils with 40 wt% mineral in Figure 3.4.2 (d) still had the lowest maximum strain, which was approximately 0.02 at 100 MPa stress. However, it should be noted that CNTs needed to compose a low weight percent of the fibril in order to provide significant reinforcement in order to decrease the fibril strain.

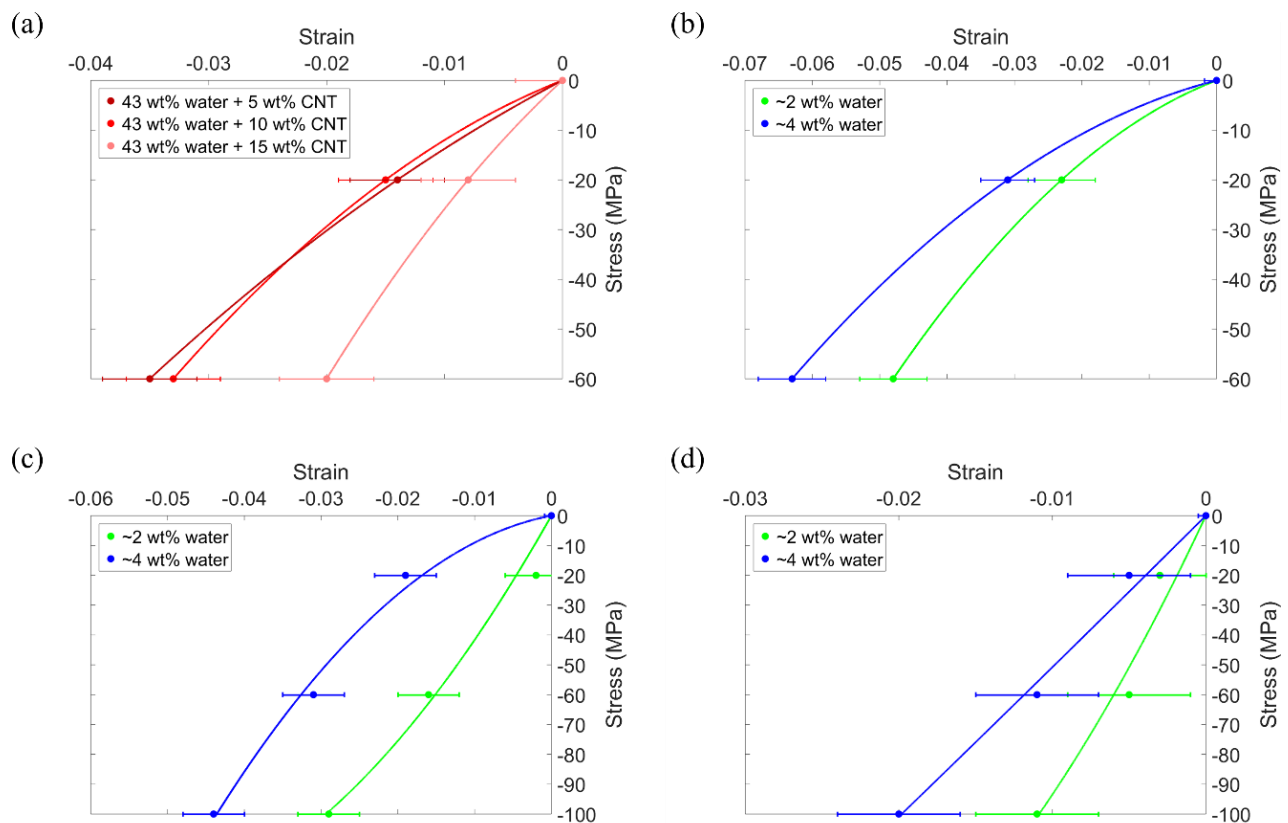


Figure 3.4.2 Compressive stress vs. strain of fibrils with CNTs (a). Also shown are fibrils with no CNTs and mineral contents of (b) 0 wt%, (c) 20 wt%, and (d) 40 wt%.

The respective Young's modulus values for the models in Figure 3.4.2 were determined and plotted in Figure 3.4.3. The fibril models from Figure 3.4.1 (a,b,c) were developed by varying the respective water and CNT concentration of fibril models developed in a previous study by Nair et al. [52]. As such, the compressive modulus determined by Nair et al. [52] were also represented in Figure 3.4.3. For non-mineralized 43 wt% hydrated fibrils, it was observed that an increase in the CNT concentration resulted in an increase in the fibril modulus. An increase in CNT concentration from 0 wt% to 15 wt% resulted in an increase in modulus from 0.43 GPa to 2.83 GPa, corresponding to an approximately 558% increase in modulus. The modulus values for the fibril/CNT composites are comparable to the modulus values of the 20 wt% mineral partially hydrated fibrils ranging from approximately 1.4 GPa to 3 GPa.

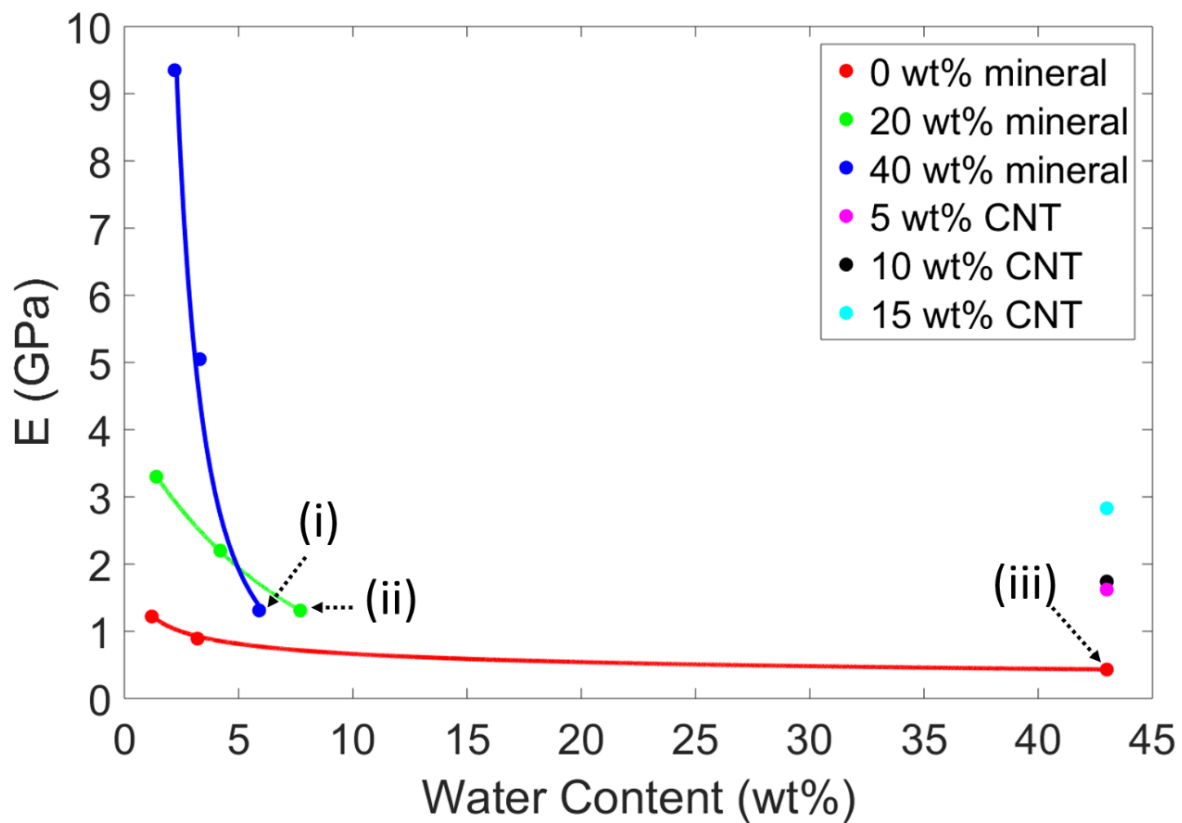


Figure 3.4.3 The compressive Young's modulus versus fibril water content for fibrils of mineral contents of 0 wt%, 20 wt% and 40 wt%. Also plotted are the Young's modulus values of non-mineralized fibrils with 43 wt% water and different CNT concentrations of 5 wt%, 10 wt%, and 15 wt%. The modulus values determined by Nair et al. [52] are also plotted as i, ii, and iii.

After analyzing the compressive modulus values of the fibrils with CNTs, investigation of the deformation mechanisms of the fibrils with CNTs was done by analyzing the fibril gap/overlap ratio. The gap/overlap ratio determined by Nair et al. [52] for non-mineralized fibrils with 43 wt% water was approximately 1.2. When 5 wt% of CNTs was added to the non-mineralized fibril with 43 wt% water, it was observed that the gap/overlap ratio increased by approximately 7%, as seen in Figure 3.4.4 (a). This was because the presence of the CNTs in the gap regions caused the gap regions to expand while the overlap region lengths remained approximately the same.

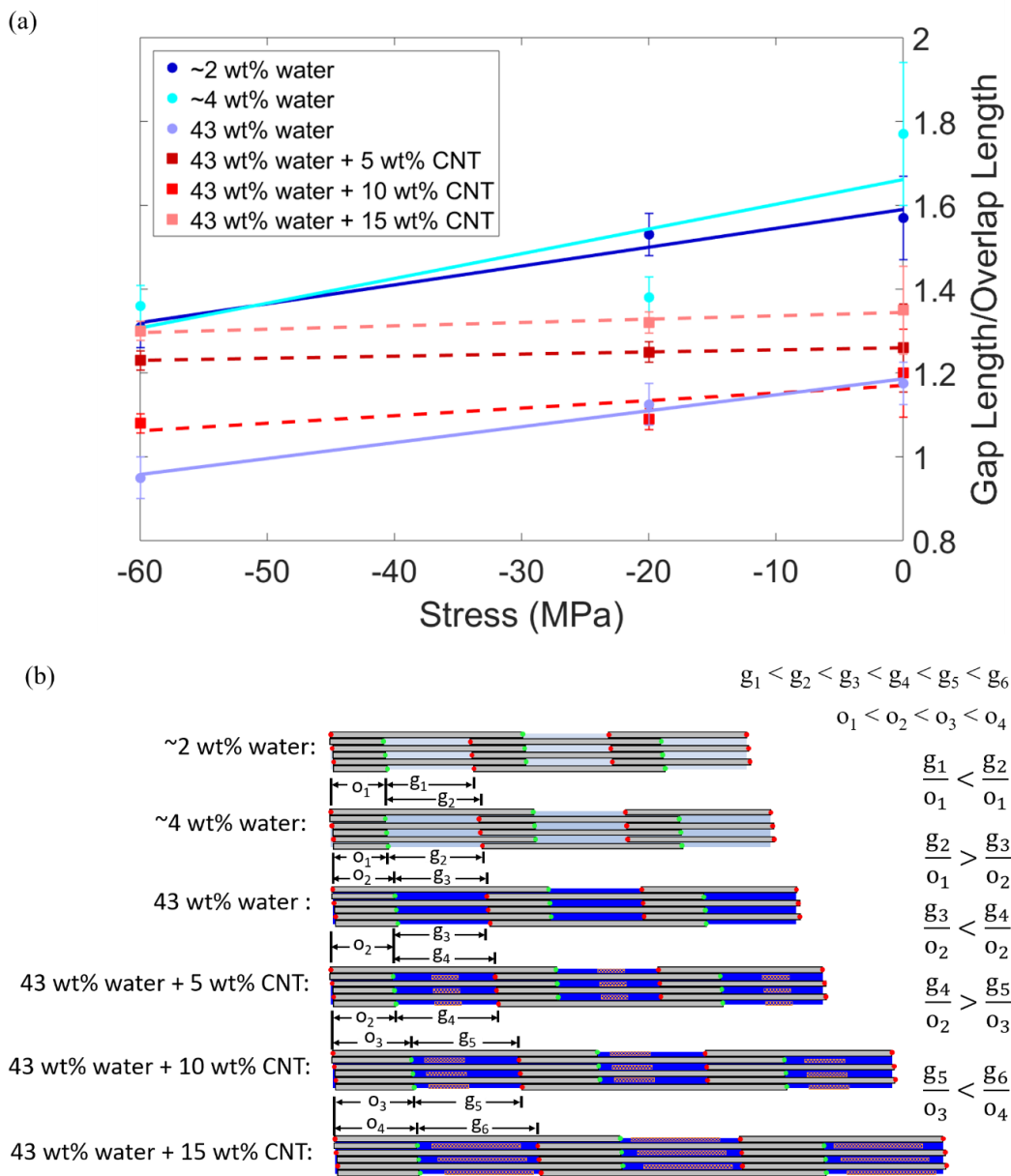


Figure 3.4.4 Gap/overlap ratio vs. compressive stress of non-mineralized fibrils (a). (b) Schematics showing the deformation of the fibril gap and overlap regions.

As the CNT concentration increased to 10 wt%, it was observed in Figure 3.4.4 that the gap/overlap ratio decreased back to approximately 1.2 when compared to the fibril with 5 wt% CNTs. This was because, while the increase in CNT concentration caused a slight expansion of the gap regions, the larger CNT concentration displaced water from the gap regions to the overlap regions which caused the overlap regions to expand. While the CNTs in the fibril with 5 wt% CNTs also caused displacement of water, the CNTs only took up approximately 28% of the gap region volume, so the displaced water remained primarily in the gap regions. The CNTs in the fibril with 10 wt% CNTs took up approximately 56% of the gap region volume, so the displaced water was primarily displaced to the overlap regions.

As the CNT concentration increased to 15 wt%, it was observed in Figure 3.4.4 that there was an approximately 13% increase in the gap/overlap ratio when compared to the fibril with 10 wt% CNTs which was observed in Figure 3.4.4 (a). At a CNT concentration of 15 wt%, the CNTs took up approximately 83% of the gap region volume, which resulted in a larger expansion of the gap regions, even though additional water was displaced to the overlap regions and caused them to slightly expand. As the stress increased, the gap/overlap ratio of the fibrils with CNTs decreased for all CNT contents. Even though the gap regions still deformed more than the overlap regions for fibrils with CNTs under compressive stress, the gap regions of fibrils with CNTs deformed less than the gap regions of fibrils without CNTs. This was seen in Figure 3.4.4 where, as the stress increased, the decrease in gap/overlap ratio for the fibrils with CNTs was less than the decrease in gap/overlap ratio for the fibrils without CNTs.

Chapter 4: Conclusions

A model of collagen fibrils with varying mineral and water content was developed and mechanically tested in tension and compression using molecular dynamics simulations. The deformation behavior of the gap/overlap regions was studied for both non-mineralized and mineralized samples. Finally, the possibility of using CNT's as a substitute for minerals in the fibrils was studied. The following conclusions were determined from analysis of the MD simulations of fibrils under tension and compression.

1. For each mineralization case in tension, the hydration of the fibrils led to the stress versus strain behavior having a more nonlinear trend. For the 0 wt% mineral and 20 wt% mineralized fibrils in compression, the stress versus strain behavior was nonlinear. An increase in the fibril water content caused the Young's modulus of the non-mineralized fibril to decrease from approximately 1.2 GPa to 0.2 GPa in tension and from approximately 1.2 GPa to 0.43 GPa in compression. In highly mineralized fibrils (40 wt%), the increase in water content resulted in a decrease in Young's modulus from approximately 1.9 GPa to 1.2 GPa in tension, and from approximately 9.4 GPa to 1.3 GPa in tension.
2. An increase in the mineral content caused the stiffness of the fibril to increase. At 0 wt% water, the tensile Young's modulus increased from approximately 1.2 GPa to 1.9 GPa when the mineral content increased from 0 wt% to 40 wt%. At 2 wt% water, the compressive Young's modulus increased from approximately 1.2 GPa to 9.4 GPa when the mineral content increased from 0 wt% to 40 wt%.
3. The inclusion of CNTs in fibrils between 5 wt% and 15 wt% increased the compressive Young's modulus of the fibrils to between 1.6 GPa to 2.8 GPa, which was comparable to the compressive modulus values of 1.3 GPa to 3.3 GPa for 20 wt% mineralized fibrils.
4. For non-mineralized fibrils, as the water content increased an expansion of the gap region

length was observed, and the gap/overlap ratio increased by as much as 40%. As the fibril water content increased from 0 wt% to ~2 wt%, the water primarily occupied voids in the gap regions. This caused the gap regions to expand and the overlap regions to contract. At a water content of 43 wt%, water was distributed uniformly throughout the fibril, which caused the overlap regions to expand.

5. As tensile stress was applied to the non-mineralized ~2 wt% hydrated fibril, the overlap regions began to expand, and the gap/overlap ratio decreased by approximately 17%.
6. For non-mineralized fibrils with ~4 wt% water, the water primarily occupied voids in the gap regions, which caused the gap region to expand. Water also occupied some voids in the overlap regions, which eliminated contraction of the overlap regions.
7. As tensile stress was applied to the non-mineralized fibril with ~4 wt% water, the gap regions deformed more than the overlap regions, and the gap/overlap ratio decreased by approximately 23%.
8. CNTs in non-mineralized fibrils with 43 wt% water occupied void space in the gap regions. The gap regions of these fibrils deformed more than the overlap regions as stress increased, with a decrease in gap/overlap ratio of approximately 6%.
9. The deformation of the gap regions of 43 wt% hydrated and non-mineralized fibrils with CNTs was less than the deformation of the gap regions of 43 wt% hydrated and non-mineralized fibrils without CNTs. The decrease in gap/overlap ratio of fibrils with CNTs was approximately 6%, while for fibrils without CNTs was approximately 19%.
10. The 10 nm long CNTs cause an expansion of the gap regions, but not the overlap regions. The 20 nm long CNTs caused an expansion of the gap regions, while the water displaced from the gap regions caused an expansion of the overlap regions that was larger than the gap regions' expansion. The 30 nm long CNTs caused an expansion of the gap regions, while the water displaced from the gap regions caused an expansion of the overlap regions that was larger than

the gap regions' expansion.

11. For 20 wt% mineralized fibrils with 0% water, as tensile stress was applied the gap/overlap ratio remained constant at approximately 1.2.
12. For 20 wt% mineralized fibrils with ~2 wt% water, the mineral in the gap regions caused the water to primarily occupy voids in the overlap regions. The water in the overlap regions caused the overlap regions to expand slightly while the gap regions contracted slightly and the gap/overlap ratio decreased to approximately 1.1. In tension, the gap regions deformed more than the overlap regions deformed as stress increased, while in compression, the overlap regions deformed more than the gap regions as stress increased.
13. For 20 wt% mineralized fibrils with ~4 wt% water, water began to also occupy some voids in the gap regions. This caused the gap regions to expand slightly, rather than contract, and the gap/overlap ratio increased to approximately 1.3.
14. For 40 wt% mineralized fibrils, as the fibril water content increased, the water was distributed uniformly throughout the fibril. However, the initial increase in water content caused the gap regions to expand slightly more than the overlap regions, and the gap/overlap ratio increased by approximately 16%.
15. As tensile or compressive stress was applied to the 40 wt% mineralized fibrils, the overlap regions deformed more than the gap regions as water in the overlap regions increased intermolecular sliding and the mineral in the gap regions resisted deformation.

References

1. Fratzl, P., *Collagen: structure and mechanics, an introduction*. Collagen: structure and mechanics, 2008: p. 1-13.
2. Saxon, S.V., M.J. Etten, and E.A. Perkins, *Physical change and aging: A guide for the helping professions*. 2014: Springer Publishing Company. pp. 37-38
3. Rauch, F. and F.H. Glorieux, *Osteogenesis imperfecta*. Lancet, 2004. **363**(9418): p. 1377-1385.
4. Mueller, K.H., A. Trias, and R.D. Ray, *Bone Density and Composition: Age-Related and Pathological Changes in Water and Mineral Content*. JBJS, 1966. **48**(1): p. 140-148.
5. Dolan, A., N. Arden, R. Grahame, and T. Spector, *Assessment of bone in Ehlers Danlos syndrome by ultrasound and densitometry*. Annals of the rheumatic diseases, 1998. **57**(10): p. 630-633.
6. Sasaki, N. and S. Odajima, *Elongation mechanism of collagen fibrils and force-strain relations of tendon at each level of structural hierarchy*. Journal of biomechanics, 1996. **29**(9): p. 1131-1136.
7. van der Rijt, J.A., K.O. van der Werf, M.L. Bennink, P.J. Dijkstra, and J. Feijen, *Micromechanical testing of individual collagen fibrils*. Macromolecular bioscience, 2006. **6**(9): p. 697-702.
8. Eppell, S., B. Smith, H. Kahn, and R. Ballarini, *Nano measurements with micro-devices: mechanical properties of hydrated collagen fibrils*. Journal of the Royal Society Interface, 2006. **3**(6): p. 117-121.
9. Minary-Jolandan, M. and M.-F. Yu, *Nanomechanical heterogeneity in the gap and overlap regions of type I collagen fibrils with implications for bone heterogeneity*. Biomacromolecules, 2009. **10**(9): p. 2565-2570.
10. Gul-E-Noor, F., C. Singh, A. Papaioannou, N. Sinha, and G.S. Boutis, *Behavior of Water in Collagen and Hydroxyapatite Sites of Cortical Bone: Fracture, Mechanical Wear, and Load Bearing Studies*. Journal of Physical Chemistry C, 2015. **119**(37): p. 21528-21537.
11. Depalle, B., Z. Qin, S.J. Shefelbine, and M.J. Buehler, *Large Deformation Mechanisms, Plasticity, and Failure of an Individual Collagen Fibril With Different Mineral Content*. Journal of Bone and Mineral Research, 2016. **31**(2): p. 380-390.
12. Gautieri, A., S. Vesentini, A. Redaelli, and M.J. Buehler, *Hierarchical structure and nanomechanics of collagen microfibrils from the atomistic scale up*. Nano letters, 2011. **11**(2): p. 757-766.
13. Nair, A.K., A. Gautieri, S.-W. Chang, and M.J. Buehler, *Molecular mechanics of mineralized collagen fibrils in bone*. Nature communications, 2013. **4**: p. 1724.

14. Streeter, I. and N.H. de Leeuw, *Atomistic Modeling of Collagen Proteins in Their Fibrillar Environment*. Journal of Physical Chemistry B, 2010. **114**(41): p. 13263-13270.
15. Tang, Y., R. Ballarini, M.J. Buehler, and S.J. Eppell, *Deformation micromechanisms of collagen fibrils under uniaxial tension*. Journal of The Royal Society Interface, 2010. **7**(46): p. 839-850.
16. Zhang, D.J., U. Chippada, and K. Jordan, *Effect of the structural water on the mechanical properties of collagen-like microfibrils: A molecular dynamics study*. Annals of Biomedical Engineering, 2007. **35**(7): p. 1216-1230.
17. Hamed, E. and I. Jasiuk, *Multiscale damage and strength of lamellar bone modeled by cohesive finite elements*. Journal of the Mechanical Behavior of Biomedical Materials, 2013. **28**: p. 94-110.
18. Ahsan, A.S., *Effect of Intrafibrillar Mineralization on the Mechanical Properties of Osteogenesis Imperfecta Bone Using a Cohesive Finite Element Approach*. 2017, The University of Texas at San Antonio.
19. Lin, L., J. Samuel, X. Zeng, and X. Wang, *Contribution of extrafibrillar matrix to the mechanical behavior of bone using a novel cohesive finite element model*. Journal of the mechanical behavior of biomedical materials, 2017. **65**: p. 224-235.
20. Thomopoulos, S., J.P. Marquez, B. Weinberger, V. Birman, and G.M. Genin, *Collagen fiber orientation at the tendon to bone insertion and its influence on stress concentrations*. Journal of Biomechanics, 2006. **39**(10): p. 1842-1851.
21. Nikolov, S. and D. Raabe, *Hierarchical modeling of the elastic properties of bone at submicron scales: The role of extrafibrillar mineralization*. Biophysical Journal, 2008. **94**(11): p. 4220-4232.
22. Hamed, E., Y. Lee, and I. Jasiuk, *Multiscale modeling of elastic properties of cortical bone*. Acta Mechanica, 2010. **213**(1-2): p. 131-154.
23. Pradhan, S.M., D.R. Katti, and K.S. Katti, *Steered molecular dynamics study of mechanical response of full length and short collagen molecules*. Journal of nanomechanics and micromechanics, 2011. **1**(3): p. 104-110.
24. Currey, J.D., *Bones: structure and mechanics*. 2002: Princeton University Press. pp. 106-107
25. Amsel, S., A. Maniatis, M. Tavassoli, and W. Crosby, *The significance of intramedullary cancellous bone formation in the repair of bone marrow tissue*. The Anatomical Record, 1969. **164**(1): p. 101-111.
26. Rockoff, S.D., E. Sweet, and J. Bleustein, *The relative contribution of trabecular and cortical bone to the strength of human lumbar vertebrae*. Calcif Tissue Res, 1969. **3**(2): p. 163-75.
27. Enlow, D.H., *Functions of the Haversian system*. Developmental Dynamics, 1962. **110**(3): p. 269-305.

28. Orgel, J.P.R.O., T.C. Irving, A. Miller, and T.J. Wess, *Microfibrillar structure of type I collagen in situ*. Proceedings of the National Academy of Sciences of the United States of America, 2006. **103**(24): p. 9001-9005.
29. Wess, T.J., A. Hammersley, L. Wess, and A. Miller, *Type-I Collagen Packing, Conformation of the Triclinic Unit-Cell*. Journal of Molecular Biology, 1995. **248**(2): p. 487-493.
30. Nudelman, F., K. Pieterse, A. George, P.H.H. Bomans, H. Friedrich, L.J. Brylka, P.A.J. Hilbers, G. de With, and N.A.J.M. Sommerdijk, *The role of collagen in bone apatite formation in the presence of hydroxyapatite nucleation inhibitors*. Nature Materials, 2010. **9**(12): p. 1004-1009.
31. Wang, Y., T. Azais, M. Robin, A. Vallee, C. Catania, P. Legriel, G. Pehau-Arnaudet, F. Babonneau, M.M. Giraud-Guille, and N. Nassif, *The predominant role of collagen in the nucleation, growth, structure and orientation of bone apatite*. Nature Materials, 2012. **11**(8): p. 724-733.
32. Timmins, P.A. and J.C. Wall, *Bone Water*. Calcified Tissue Research, 1977. **23**(1): p. 1-5.
33. Nyman, J.S., A. Roy, X.M. Shen, R.L. Acuna, J.H. Tyler, and X.D. Wang, *The influence of water removal on the strength and toughness of cortical bone*. Journal of Biomechanics, 2006. **39**(5): p. 931-938.
34. Tanaka, M., Y. Sato, M. Zhang, H. Haniu, M. Okamoto, K. Aoki, T. Takizawa, K. Yoshida, A. Sobajima, and T. Kamanaka, *In Vitro and In Vivo Evaluation of a Three-Dimensional Porous Multi-Walled Carbon Nanotube Scaffold for Bone Regeneration*. Nanomaterials, 2017. **7**(2): p. 46.
35. Hirata, E., M. Uo, H. Takita, T. Akasaka, F. Watari, and A. Yokoyama, *Multiwalled carbon nanotube-coating of 3D collagen scaffolds for bone tissue engineering*. Carbon, 2011. **49**(10): p. 3284-3291.
36. Amirian, M., A.N. Chakoli, J.H. Sui, and W. Cai, *Enhanced mechanical and photoluminescence effect of poly (L-lactide) reinforced with functionalized multiwalled carbon nanotubes*. Polymer bulletin, 2012. **68**(6): p. 1747-1763.
37. MacDonald, R.A., B.F. Laurenzi, G. Viswanathan, P.M. Ajayan, and J.P. Stegemann, *Collagen-carbon nanotube composite materials as scaffolds in tissue engineering*. Journal of Biomedical Materials Research Part A, 2005. **74**(3): p. 489-496.
38. Zanello, L.P., B. Zhao, H. Hu, and R.C. Haddon, *Bone cell proliferation on carbon nanotubes*. Nano letters, 2006. **6**(3): p. 562-567.
39. Meng, J., H. Kong, Z. Han, C. Wang, G. Zhu, S. Xie, and H. Xu, *Enhancement of nanofibrous scaffold of multiwalled carbon nanotubes/polyurethane composite to the fibroblasts growth and biosynthesis*. Journal of Biomedical Materials Research Part A, 2009. **88**(1): p. 105-116.
40. Jing, Z., Y. Wu, W. Su, M. Tian, W. Jiang, L. Cao, L. Zhao, and Z. Zhao, *Carbon nanotube reinforced collagen/hydroxyapatite scaffolds improve bone tissue formation in vitro and in vivo*. Annals of biomedical engineering, 2017. **45**(9): p. 2075-2087.

41. Silva, E., L.M.R. de Vasconcellos, B.V. Rodrigues, D.M. dos Santos, S.P. Campana-Filho, F.R. Marciano, T.J. Webster, and A.O. Lobo, *PDLLA honeycomb-like scaffolds with a high loading of superhydrophilic graphene/multi-walled carbon nanotubes promote osteoblast in vitro functions and guided in vivo bone regeneration*. *Materials Science and Engineering: C*, 2017. **73**: p. 31-39.
42. He, H., L.A. Pham-Huy, P. Dramou, D. Xiao, P. Zuo, and C. Pham-Huy, *Carbon nanotubes: applications in pharmacy and medicine*. *BioMed Research International*, 2013. **2013**.
43. Qin, L.-C., *Determination of the chiral indices (n, m) of carbon nanotubes by electron diffraction*. *Physical Chemistry Chemical Physics*, 2007. **9**(1): p. 31-48.
44. Zhang, P., Y. Huang, P. Geubelle, P. Klein, and K. Hwang, *The elastic modulus of single-wall carbon nanotubes: a continuum analysis incorporating interatomic potentials*. *International Journal of Solids and Structures*, 2002. **39**(13): p. 3893-3906.
45. Yamago, S., Y. Watanabe, and T. Iwamoto, *Synthesis of [8]cycloparaphenylene from a square-shaped tetranuclear platinum complex*. *Angew Chem Int Ed Engl*, 2010. **49**(4): p. 757-9.
46. Charlier, J., P. Lambin, and T.W. Ebbesen, *Electronic properties of carbon nanotubes with polygonized cross sections*. *Phys Rev B Condens Matter*, 1996. **54**(12): p. R8377-R8380.
47. Balandin, A.A., *Thermal properties of graphene and nanostructured carbon materials*. *Nat Mater*, 2011. **10**(8): p. 569-81.
48. Kang, Y., Q. Wang, Y.C. Liu, T. Wu, Q. Chen, and W.J. Guan, *Dynamic mechanism of collagen-like peptide encapsulated into carbon nanotubes*. *The Journal of Physical Chemistry B*, 2008. **112**(15): p. 4801-7.
49. Bala, Y. and E. Seeman, *Bone's Material Constituents and their Contribution to Bone Strength in Health, Disease, and Treatment*. *Calcified Tissue International*, 2015. **97**(3): p. 308-326.
50. MacKerell Jr, A.D., D. Bashford, M. Bellott, R.L. Dunbrack Jr, J.D. Evanseck, M.J. Field, S. Fischer, J. Gao, H. Guo, and S. Ha, *All-atom empirical potential for molecular modeling and dynamics studies of proteins*. *The Journal of Physical Chemistry B*, 1998. **102**(18): p. 3586-3616.
51. Plimpton, S., *Fast Parallel Algorithms for Short-Range Molecular-Dynamics*. *Journal of Computational Physics*, 1995. **117**(1): p. 1-19.
52. Nair, A.K., A. Gautieri, and M.J. Buehler, *Role of intrafibrillar collagen mineralization in defining the compressive properties of nascent bone*. *Biomacromolecules*, 2014. **15**(7): p. 2494-2500.
53. Shi, X., B. Sitharaman, Q.P. Pham, F. Liang, K. Wu, W.E. Billups, L.J. Wilson, and A.G. Mikos, *Fabrication of porous ultra-short single-walled carbon nanotube nanocomposite scaffolds for bone tissue engineering*. *Biomaterials*, 2007. **28**(28): p. 4078-4090.

54. Sitharaman, B., X. Shi, X.F. Walboomers, H. Liao, V. Cuijpers, L.J. Wilson, A.G. Mikos, and J.A. Jansen, *In vivo biocompatibility of ultra-short single-walled carbon nanotube/biodegradable polymer nanocomposites for bone tissue engineering*. Bone, 2008. **43**(2): p. 362-370.
55. Sun, X., S. Zaric, D. Daranciang, K. Welsher, Y. Lu, X. Li, and H. Dai, *Optical properties of ultrashort semiconducting single-walled carbon nanotube capsules down to sub-10 nm*. Journal of the American Chemical Society, 2008. **130**(20): p. 6551-6555.
56. Javey, A., J. Guo, M. Paulsson, Q. Wang, D. Mann, M. Lundstrom, and H. Dai, *High-field quasiballistic transport in short carbon nanotubes*. Physical Review Letters, 2004. **92**(10): p. 106804.
57. Tan, W., J. Twomey, D. Guo, K. Madhavan, and M. Li, *Evaluation of nanostructural, mechanical, and biological properties of collagen–nanotube composites*. IEEE Transactions on Nanobioscience, 2010. **9**(2): p. 111-120.
58. Samuel, J., J.-S. Park, J. Almer, and X. Wang, *Effect of water on nanomechanics of bone is different between tension and compression*. Journal of the Mechanical Behavior of Biomedical Materials, 2016. **57**: p. 128-138.
59. Uhlig, M.R. and R. Magerle, *Unraveling capillary interaction and viscoelastic response in atomic force microscopy of hydrated collagen fibrils*. Nanoscale, 2017. **9**(3): p. 1244-1256.
60. Hang, F. and A.H. Barber, *Nano-mechanical properties of individual mineralized collagen fibrils from bone tissue*. Journal of the Royal Society Interface, 2011. **8**(57): p. 500-505.
61. Gao, H., B. Ji, I.L. Jäger, E. Arzt, and P. Fratzl, *Materials become insensitive to flaws at nanoscale: lessons from nature*. Proceedings of the national Academy of Sciences, 2003. **100**(10): p. 5597-5600.
62. Jäger, I. and P. Fratzl, *Mineralized collagen fibrils: a mechanical model with a staggered arrangement of mineral particles*. Biophysical journal, 2000. **79**(4): p. 1737-1746.
63. Grant, C.A., D.J. Brockwell, S.E. Radford, and N.H. Thomson, *Effects of hydration on the mechanical response of individual collagen fibrils*. Applied Physics Letters, 2008. **92**(23): p. 233902.
64. Kemp, A.D., C.C. Harding, W.A. Cabral, J.C. Marini, and J.M. Wallace, *Effects of tissue hydration on nanoscale structural morphology and mechanics of individual Type I collagen fibrils in the Brtl mouse model of Osteogenesis Imperfecta*. Journal of Structural Biology, 2012. **180**(3): p. 428-438.
65. Lefèvre, E., C. Guivier-Curien, M. Pithioux, and A. Charrier, *Determination of mechanical properties of cortical bone using AFM under dry and immersed conditions*. Computer Methods in Biomechanics and Biomedical Engineering, 2013. **16**(sup1): p. 337-339.
66. Dubey, D.K. and V. Tomar, *The effect of tensile and compressive loading on the hierarchical strength of idealized tropocollagen–hydroxyapatite biomaterials as a function of the chemical environment*. Journal of Physics: Condensed Matter, 2009. **21**(20): p. 205103.

67. Karunaratne, A., C.R. Esapa, J. Hiller, A. Boyde, R. Head, J. Bassett, N.J. Terrill, G.R. Williams, M.A. Brown, and P.I. Croucher, *Significant deterioration in nanomechanical quality occurs through incomplete extrafibrillar mineralization in rachitic bone: Evidence from in-situ synchrotron X-ray scattering and backscattered electron imaging*. Journal of Bone and Mineral Research, 2012. **27**(4): p. 876-890.
68. Ji, B., H. Gao, and K. Jimmy Hsia, *How do slender mineral crystals resist buckling in biological materials?* Philosophical Magazine Letters, 2004. **84**(10): p. 631-641.
69. Li, C. and T.-W. Chou, *A structural mechanics approach for the analysis of carbon nanotubes*. International Journal of Solids and Structures, 2003. **40**(10): p. 2487-2499.
70. Lu, J.P., *Elastic properties of carbon nanotubes and nanoropes*. Physical Review Letters, 1997. **79**(7): p. 1297.
71. Popov, V., V. Van Doren, and M. Balkanski, *Elastic properties of single-walled carbon nanotubes*. Physical Review B, 2000. **61**(4): p. 3078.
72. Hernandez, E., C. Goze, P. Bernier, and A. Rubio, *Elastic properties of C and B x C y N z composite nanotubes*. Physical Review Letters, 1998. **80**(20): p. 4502.
73. Salvetat, J.-P., G.A.D. Briggs, J.-M. Bonard, R.R. Bacsa, A.J. Kulik, T. Stöckli, N.A. Burnham, and L. Forró, *Elastic and shear moduli of single-walled carbon nanotube ropes*. Physical review letters, 1999. **82**(5): p. 944.
74. Krishnan, A., E. Dujardin, T. Ebbesen, P. Yianilos, and M. Treacy, *Young's modulus of single-walled nanotubes*. Physical review B, 1998. **58**(20): p. 14013.

Appendix A: Description of Research for Popular Publication

A Computational Study of the Effects of Mineral, Water, and Carbon Nanotube Content on the Nanoscale Behavior of Bone

Bone is a composite biomaterial that provides structure and support for the body. However, different conditions can reduce bone's ability to provide this structure and support. For example, studies have shown that as people age the mineral content and water content of their bones decreases and the likelihood of their bones fracturing increases. Other factors include diseases and genetic conditions, such as osteoporosis and brittle bone disease which make bones more brittle and increase the likelihood of bone fracture. Ehler's-Danlos syndrome is a genetic condition that causes a person's skin, joints, and bones to become hyperflexible. Understanding how bone's mechanical properties change is important for developing detection and treatment methods for these conditions that negatively affect bones structure and support ability. For example, some treatment methods include scaffolds for tissue engineering in wound healing, or bone implants. Understanding these properties at the nanoscale, a size scale that is smaller than what is visible to the human eye, is important for the development of early detection and treatment methods of conditions that negatively affect bone. At the nanoscale, bone is primarily composed of small fibers known as fibrils that are a composite of collagen protein, apatite mineral, and water. The collagen protein molecules align themselves in a staggered fashion to form what are known as "gap" and "overlap" regions, with the mineral and water filling the voids between the collagen molecules.

Several studies have found that carbon nanotubes are a promising material to include in scaffolds for bone tissue engineering, or in bone implants. Though several studies have characterized nanoscale bone properties as the mineral content changes, the effect of water, mineral, and carbon nanotube (CNT) content and distribution in bone at the nanoscale is unexplored. This study used

molecular dynamics simulations to investigate how collagen fibril deformation behavior changed as the fibril mineral, water, and CNT content changed. Collagen fibrils with 0 wt%, 20 wt%, and 40 wt% mineral and 0 wt%, 2 wt%, and 4 wt% water were studied for fibrils pulled in tension or when compressed. Non-mineralized fibrils with 43 wt% water and 5 wt%, 10 wt%, and 15 wt% CNTs were also studied under compression. This study found that an increase in mineral content for hydrated fibrils was found to reduce the nonlinear stress versus strain behavior caused by hydration, and the stiffness of non-mineralized and mineralized fibrils decreased as the water content increased.

Mineral and water content were found to affect the distribution of water in fibrils in tension and compression, which changed the deformation behavior of the gap and overlap regions. An increase in water content was found to increase the ratio of gap region length to overlap region length (gap/overlap ratio) by as much as 40% in non-mineralized fibrils and 16% in mineralized fibrils. For non-mineralized fibrils it was found that the gap/overlap ratio increased as the applied stress increased, while in mineralized fibrils the gap/overlap ratio decreased with an increase in stress. This showed that the presence of mineral changes whether the gap regions or overlap regions deform more. CNTs in non-mineralized fibril gap region voids also reduced the deformation of the fibril gap regions. This meant that the CNTs also had the effect of increasing the non-mineralized fibril stiffness (elastic modulus) from 0.43 GPa to approximately to 2.83 GPa, which was comparable to the stiffness of mineralized fibrils.

This study has shown that the interaction between mineral, water, and CNTs plays a crucial role in the mechanical behavior of collagen fibrils. This is important for understanding how the nanoscale properties of bone change when conditions affect its mineral and water content. The results of this study are also important for the development of bone tissue engineering scaffolds for bone implants or application in wound healing materials, whose properties can change based on the material mineral, water, or CNT content.

Appendix B: Executive Summary of Newly Created Intellectual Property

The novelty in this study determined mechanical properties of collagen fibrils, which are the material component of bone at the nanoscale. The collagen fibrils were studied under different physiological conditions corresponding to fibril mineral, water, and carbon nanotube content.

This study used established open source models of collagen fibrils validated by experiment. This study also used established and open source molecular dynamics methods and software to perform tensile and compressive tests on collagen fibrils. As such, while discovery of new results was made of the mechanical properties of collagen fibrils under different physiological conditions, no new intellectual property was created.

Appendix C: Potential Patent and Commercialization Aspects of Intellectual Property

C.1 Patentability of Intellectual Property (Could Each Item be Patented)

While novel results were found in the study, no intellectual property was developed by way of novel collagen fibril models or by MD simulation techniques for tension or compression tests. Since no new intellectual property was created, there is no available patentable intellectual property from this study.

C.2 Commercialization Prospects (Should Each Item be Patented)

Not applicable

C.3 Possible Prior Disclosure of IP

Not applicable

Appendix D: Broader Impact of Research

D.1 Applicability of Research Methods to Other Problems

The results of this study can be used to guide the development of bio-inspired materials, scaffolds for tissue engineering, and bone implants. These would be scaffolds or implants whose material components consist of collagen protein, HAP mineral, or ultra-short CNTs. Further work could also expand the current fibril model to study the effects of bound water, mineral substitution, apatite crystal size, or other variables on the mechanical behavior of collagen fibrils. The results of this study could also be used to refine the model of collagen fibrils developed by Gao et al.

D.2 Impact of Results Research on Global and U.S. Society

As mentioned in section D.1, the results of this study could be used to develop scaffolds for tissue engineering, and bone implants in order to better treat bone conditions. Understanding the effect of mineral, water, or CNT content on the mechanical behavior of collagen fibrils is useful as a guide to optimize tissue scaffolds or implants made of these materials. This optimization would be making the scaffolds or implants more biocompatible to the tissue it is replacing by having the scaffold or implant mechanical properties matched as closely as possible to the mechanical properties of the tissue it is replacing.

D.3 Impact of Research Results on the Environment

Collagen fibrils are a biological material, and as such are not harmful to the human body or to the environment. The specific inclusion of CNTs in tissue engineering scaffolds have found that ultra-short CNTs are safely degradable and eliminable in the human body, as referenced in Section 2.5.

Appendix E: Microsoft Project for MS Microelectronics-Photonics Degree Plan

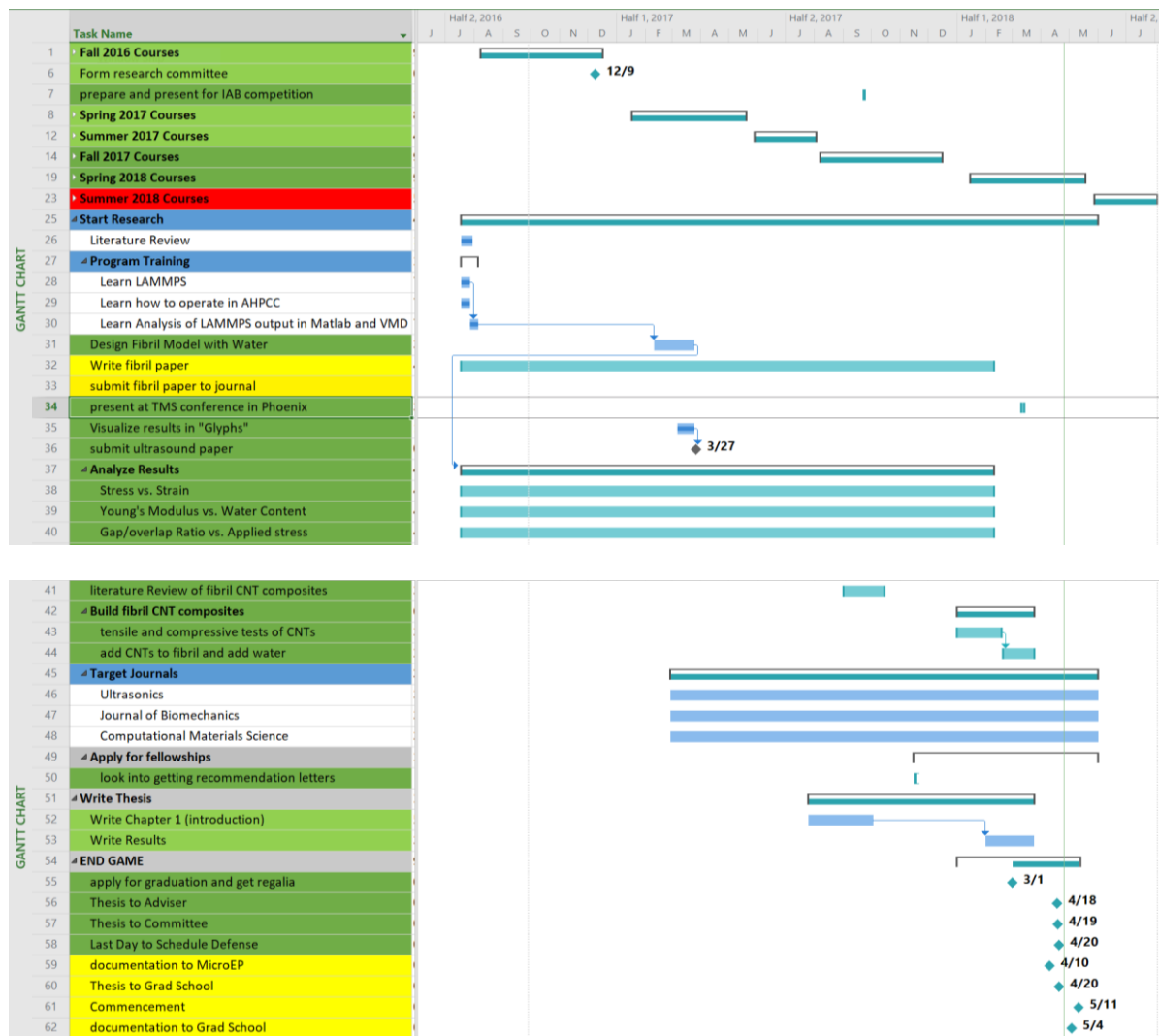


Figure A.1. Microsoft Project for Marco Fielder for the Microelectronics-Photonics Degree Plan

Appendix F: Identification of Software Used in Research and Thesis

Computer #1

Device name: MEEG – D081

Location: NANO 112B

Owner: University of Arkansas

Computer #2: Personal laptop

Device name: DESKTOP – IVN63CK

Device owner: Marco Fielder

Software #1:

Name: LAMMPS (open source)

Downloaded by: Marco Fielder

Software #2:

Name: Microsoft Office 2016

Purchased by: University of Arkansas

Software #3:

Name: MATLAB

Purchased by: University of Arkansas

Software #4:

Name: VMD (open source)

Downloaded by: Marco Fielder

Software #5:

Name: EndNote

Purchased by: Multiscale Materials Modeling Laboratory, University of Arkansas

Appendix G: All Publications Published, Submitted, and Planned

Marco Fielder and Nair, AK., *Effects of Hydration and Intrafibrillar Mineralization on the Mechanical Behavior of Collagen Fibrils in Tension*. Biomechanics and Modeling in Mechanobiology (in submission)

Marco Fielder and Nair, AK., *A Computational Study of the Impact of Intrafibrillar Mineral, Water, and Carbon Nanotube Content on the Mechanical Behavior of Collagen Fibrils in Compression*. (in preparation)